Alma Mater Studiorum – Università di Bologna

DOTTORATO DI RICERCA IN

COMPUTER SCIENCE AND ENGINEERING

Ciclo XXXI

Settore Concorsuale: 09/H1

Settore Scientifico Disciplinare: ING-INF/05

A fully-wearable non-invasive SSVEP-based BCI system enabled by AR techniques for daily use in real environment.

Presentata da: Mattia Salvaro

Coordinatore Dottorato

Prof. Paolo Ciaccia

Supervisore

Prof. Michela Milano

Co-supervisore

Prof. Luca Benini

Esame finale anno 2019

ALMA MATER STUDIORUM - UNIVERSITY OF BOLOGNA

A fully-wearable non-invasive SSVEP-based BCI system enabled by AR techniques for daily use in real environment.

by

Mattia Salvaro

A thesis submitted for the degree of
Doctor of Philosophy

in the
Faculty of Engineering
Department of Computer Science and Engineering (DISI)

February 2019

"If we knew what it was we were doing, it would not be called research, would it?"

Albert Einstein

ALMA MATER STUDIORUM - UNIVERSITY OF BOLOGNA

Abstract

Faculty of Engineering
Department of Computer Science and Engineering (DISI)

Doctor of Philosophy

by Mattia Salvaro

This thesis aims to explore the design and implementation of Brain Computer Interfaces (BCIs) specifically for non medical scenarios, and therefore to propose a solution that overcomes typical drawbacks of existing systems such as long and uncomfortable setup time, scarce or nonexistent mobility, and poor real-time performance. The research starts from the design and implementation of a plug-and-play wearable low-power BCI that is capable of decoding up to eight commands displayed on a LCD screen, with about 2 seconds of latency. The thesis also addresses the issues emerging from the usage of the BCI during a walk in a real environment while tracking the subject via indoor positioning system. Furthermore, the BCI is then enhanced with a smart glasses device that projects the BCI visual interface with augmented reality (AR) techniques, unbinding the system usage from the need of infrastructures in the surrounding environment.

Acknowledgements

I would like to thank my advisors, Michela Milano and Luca Benini, for giving me the opportunity to pursue this PhD, my supervisors at Micrel Lab Simone Benatti and Marco Guermandi, and my lab fellows Victor Kartsch, Fabio Montagna, Hanie Aghazadeh, Tommaso Polonelli and Alberto Girolami. It has been very nice to share this experience with all of you.

I would also like to thank my supportive family, to which I owe this achievement, and my girlfriend Manuela, that helped me a lot through thick and thin.

Contents

List of Figures

List of Tables

Abbreviations

ADC	**A**nalog-to-**D**igital **C**onverter
AFE	**A**nalog **F**ront **E**nd
ANN	**A**rtificial **N**eural **N**etwork
AR	**A**ugmanted **R**eality
ASL	**A**myotrophic **L**ateral **S**clerosis
BCI	**B**rain **C**omputer **I**nterface
BMI	**B**rain **M**achine **I**nterface
CCA	**C**anonical **C**orrelation **A**nalysis
CPS	**C**yber **P**hysical **S**ystem
DSP	**D**igital **S**ignal **P**rocessing
ECoG	**E**lectro**C**orticO**G**raphy
EEG	**E**lectro**E**ncephalo**G**raphy
EMG	**E**lectro**M**yo**G**ram
EOG	**E**lectro**O**culo**G**raphy
fMRI	**f**unctional **M**agnetic **R**esonance **I**maging
FFT	**F**ast **F**ourier **T**ransform
FPU	**F**loating **P**oint **U**nit
FTA	**F**requency **T**agging **A**nalysis
HCI	**H**uman **C**omputer **I**nterface
HMI	**H**uman **M**achine **I**nterface
HMD	**H**ead-**M**ounted **D**isplay
GUI	**G**raphic **U**ser **I**nterface
GPS	**G**lobal **P**ositioning **S**ystem
IEEG	**I**ntracranial **EEG**
IDE	**I**ntegrated **D**evelopment **E**nvironment

IoT	**I**nternet **o**f **T**hings
ITR	**I**nformation **T**ransfer **R**ate
LBS	**L**ocation-**B**ased **S**ervice
LDA	**L**inear **D**iscriminant **A**nalysis
LED	**L**ight **E**mitting **D**iode
MEG	**M**agneto**E**ncephalo**G**raphy
MFD	**M**atched **F**ilter **D**etector
PCA	**P**rincipal **C**omponent **A**nalysis
PCB	**P**rinted **C**ircuit **B**oard
PLI	**P**ower **L**ine **I**nterference
PSD	**P**ower **S**pectral **D**ensity **A**nalysis
RFID	**R**adio **F**requency **ID**entification
SCP	**S**low **C**ortical **P**otential
SPI	**S**erial **P**eripheral **I**nterface
SVD	**S**ingular **V**alue **D**ecomposition
SVM	**S**upport **V**ector **M**achine
SSVEP	**S**teady **S**tate **VEP**
TRCA	**T**ask **R**elated **C**omponent **A**nalysis
TVEP	**T**ransient **VEP**
SNR	**S**ignal-to-**N**oise **R**atio
UWB	**U**ltra **W**ide **B**and
VEP	**V**isual **E**voked **P**otential

To my family.

Chapter 1

Introduction

Interaction with machines and electronic systems has become more and more frequent and well-established since the third industrial revolution, often referred to as digital revolution, starting from the second half of the 20th century. During this time, the adoption and proliferation of digital computers marked the beginning of the Information Age, which still continues to the present days. To control those electronic systems several paradigms of Human Machine Interactions (HMIs) have been developed during the years, starting from the keyboard based command line, to the more recent vocal interface, passing through Graphic User Interfaces (GUIs) and touch screen. The fourth industrial revolution, started in the beginning of the 21st century, pushed the capabilities of electronic systems even farther thanks to the miniaturization of powerful and power efficient computational and communication units. The ability of decentralize computation near sensor and the empowered communication are key factors for the rise of technologies such as Internet of Things (IoT), Cyber Physical Systems (CPSs) and cloud computing. In industry, the exploitation of these new technologies is generically called Industry 4.0, where benefits are achieved through CPSs that create virtual representation of the physical production processes and are able to take autonomous decentralized decisions or communicate and cooperate with each other at both internal and inter-company level.

The digital revolution reflects in the mass market with products like smartphones, smartwatches, wristbands and any kind of wearable device capable of short range or long range communication. Along with new devices development, also new and smarter HMI paradigms have been devised that exploit the device internal sensors to detect user commands (e.g. step counter for smartphones, or wrist rotation for smartwatches). Other devices exploit biosignals for user interaction like Myo Armband [2], which is able to sense Electromyogram (EMG) of the forearm muscles and translates the signal

into commands. Brain Computer Interfaces (BCIs), also known as Brain Machine Interfaces (BMIs), are a particular type of HMIs that exploit brain activity signals acquired via Electroencephalography (EEG). BCIs were first developed to support people with disabilities in their interaction with the external world, with one of the first successful examples being BCI spellers. Recent years have seen BCI applications reach out to a larger set of scenarios, such as industry, gaming, learning, healthcare [3] and rehabilitation [4]. Several tech companies developing consumer-oriented products (Google, Apple, Facebook, etc.) have also become active in this field [5–7], with the vision of being able to substitute traditional HMIs based on conventional computer input devices, gesture and voice recognition, touch-screen interaction [2, 8, 9], with the possibility to directly interact and control computers with our brain.

Bringing this fascinating idea into life will be a tremendous boost towards integrating actions and interactions with objects in a fully-connected IoT scenario. Applications can range from verifying whether a worker is attending a specific task or effectively receiving a communication for safety purposes, to remotely control devices in industrial or home environments, to navigating menus in shops or restaurants, to gaming. These applications have different requirements as compared to traditional BCI spellers. On the one hand, they mostly require less symbols to be recognized with respect to a full speller, on the other hand they need system latencies to be minimized, both in setup time and real-time performance. However, traditional BCI systems suffer from a certain complexity, cost and size, which can only be reduced by moving processing to an external hardware, compromising portability and ease-of-use.

The foundation of every BCI system lies in the acquisition of signals that relates to brain activity. Among the available techniques to extract such information, EEG is considered as the ideal (if not the only) candidate for consumer applications and has enjoyed significant improvements in recent years. What was once possible only through expensive and cumbersome devices, it is now available on the market in cheap and relatively attractive form-factors. Most of them are conceived for gaming and entertainment or leisure, like MindMaze Mask [10], Neurosky MindWave [11], and Emotiv Insight and EPOC+ [12]. Not all these systems can acquire EEG with the same signal quality and setup complexity (i.e. number and type of electrodes), resulting in different BCI ease-of-use and performance. Moreover, these consumer products are conceived to be more a toy that identifies mood, focus, meditation, or facial expression of the user, rather than an actual machine communication tool. Only few commercial products are designed for custom BCI application development, OpenBCI [13] for example offers an open source platform for biosignals (mainly EEG) acquisition and streaming, while g.tec Intendix [14] provides a full PC based BCI speller. A common drawback of these systems is that they require a continuous data-link between on-body sensors and mobile phones/tablets, or laptop computers and workstations. This impairs some important features such as

wearability and minimal intrusiveness, increasing overall system cost as well. Moreover, it causes a severe reduction of the energy efficiency of the whole system [15–17] as it requires transmission of non-negligible amounts of data. To avoid these issues, the digital processing should be moved near-sensor, executing algorithms directly on the wearable device [18, 19]. Such solutions are not readily available, both in commercial systems and research literature. The focus of this work is to build and validate a BCI system that fulfill desirable features such as wearability, power efficiency, fast setup, stand-alone, fast responsiveness. The next section depicts in more detail what are the original contribution of this thesis.

1.1 Thesis contribution

In an effort to provide a BCI system better tailored for the new scenarios that are envisioned for the near future, this work proposes three major contributions. The first one is the design and implementation of an embedded, minimally invasive, low-power, low-cost, asynchronous BCI speller, able to recognize up to eight different stimuli with an information transfer rate (ITR) of more than 1 b/s with zero-preparation time thanks to the usage of dry electrodes. This is comparable with state-of-the-art non-wearable systems (where signal processing is computed on external hardware), thanks to careful optimization of the processing and pre-processing algorithms, which are specifically tailored on the proposed system configuration. The second contribution is the assessment of the wearable BCI in a task that implies user navigation, binding the EEG response with the position of the subject, in order to understand the challenges of the acquisition of EEG signals (artifacts, external noise and hardware constrains) in real environments, and to study the correlations between the brain activity and the subject's location or movements. The final contribution is the enhancement of the proposed wearable BCI system with a Head-Mounted Display (HMD) that provides visual stimuli through Augmented Reality techniques (AR), achieving 80% accuracy with average latency of 3 seconds and allowing for a fully wearable fast and reliable BCI system. The structure of this thesis will follow the order of the three main contributions stated above.

Chapter 2

Brain Computer Interface

2.1 Overview

Brain Computer Interfaces (BCIs) are hardware-software systems that enables human machine communication without need of muscles or peripheral nerves, exploiting exclusively electroencephalographic activity (EEG) as control signals [20]. BCI systems are typically composed by a signal acquisition headset and a signal processing device, and optionally feature an input stimuli presentation system and an output display or actuator. BCI systems recognize patterns in EEG signal following five stages: signal acquisition, signal enhancement or preprocessing, features extraction, classification, control interface [21]. The underlying implementation of the five stages are driven by design goals including target application and users, form factor, type of brain activity leveraged, and desired target performance.

Decoding brain signal is a very challenging task. In fact, the control signal is captured together with other signals from other brain activities that may overlap in time and space. Further noise can be added by artifacts due to muscular and ocular movements, generating a different type of signal measurable by techniques such as electromyography (EMG) and electroculography (EOG). Both EMG and EOG signals are present in some areas of the head where EEG is also observable, interfering with EEG acquisition. In addition, the amplitude of the EEG signal can be more or less diminished according to the type of acquisition system adopted. In *invasive* BCI systems, microelectrode arrays are physically implanted in the cerebral cortex, the implant requires brain surgery and is therefore prerogative of very specific experimental medical settings. This technique is called electrocorticography (ECoG), and compared to EEG it provides better SNR, since it avoids artifacts like eye blinking or movements and it is more spatially accurate since the electrodes are physically attached to the signal source area. On the other hand,

non-invasive BCI systems use removable electrodes applied on the scalp, where the EEG signal is diminished and spread on a wider area, resulting in more noisy and overlapping signals, but at the same time providing a more appealing setup for non-medical scenarios, allowing BCIs to steer towards consumer market for everyday use. A more detailed taxonomy of existing BCI systems is illustrated in Sec 2.3.

BCI systems also differ with respect to the type of control signals they work with. Modern BCI systems rely on five different types of brain activity: Slow Cortical Potentials (SCPs), neuronal action potentials, sensorymotor rhythms, P300 evoked potentials, and Visual Evoked Potentials (VEPs) [1, 22]. SCPs are slow voltage changes that occur in cortex and can last from 0.5 s to 10 s. Positive SCPs are associated to decreased activity in neurons, while negative SCPs are associated with neuronal activity. It has been shown by [23–25] that properly trained people can control their SCPs, and therefore it is possible for them to control cursor movement on a computer screen. Neuronal action potentials are measured in an invasive way, using cone electrodes inserted in the motor cortex. The electrodes sense the single cortical neuron-induced potential, however, unlike SCPs, these potential are more difficult to control and the need for continuous medication has hindered the popularity of this technique. Sensorymotor rhythms are a combination of mu and beta rhythms (see Sec. 2.2.1) and are associated with motor imagery, without any actual movement [26]. Once again, user training is necessary to emphasize kinesthetic experiences rather than the visual representation of the movements [1]. P300 evoked potentials are potential peaks found in an EEG related to infrequent stimuli of visual, auditory or somatosensory type. The peak is measured around 300 ms after the infrequent stimulus onset, and its amplitude grows inversely with the frequency of the stimulus. P300 has been widely used for both medical and non-medical BCI systems thanks to its relatively fast outcome and because it does not need any user training. Typical P300-based BCI applications are spellers, where letters and symbols are presented to the user in a matrix form and sequentially highlighted. The specific highlighting sequence may affect the BCI performance and it is part of its design. Typically, P300-based BCIs use the average of several trials of the infrequent stimulus in order to increase accuracy. VEPs are electrical potentials evoked in the visual cortex by visual stimuli, similarly to visual P300. The difference between visual P300 and VEP is that while P300 is evoked by an infrequent and possibly unpredictable stimulus, VEP is evoked by periodic repetitions of the same stimulus. VEPs can be divided into Transient VEPs (TVEPs) and Steady State VEPs (SSVEPs), where the discriminating factor is the frequency of the repetition. According to [27], TVEPs are bounded to frequencies lower than 4 Hz, while [28] reduces the threshold frequency to 2 Hz. However, the two authors agree in setting at 6 Hz the lower bound for SSVEPs frequency. From the neurological point of view, TVEPs show a resting phase between two consecutive repetitions, while SSVEPs are overlapped. In practice, the detection of

TVEPs and SSVEPs requires the same kind of processing, and the two techniques can be basically considered as one. VEPs, together with P300, are the most used techniques for medical and non-medical BCIs. Like P300, VEP requires no training, but it has been shown to be faster [29]. As a drawback, the signal is usually very noisy, since its acquisition is performed in a non-invasive fashion, and the amplitude and phase of the VEP is very sensitive to stimulus parameters such as frequency and contrast.

The lack of a common evaluation framework for BCI systems caused the adoption of heterogeneous performance metrics. In literature, it is possible to find assessment of BCIs made on different metrics, usually reflecting the particular BCI application metric. As a result, it is sometimes hard, or even impossible, to compare BCIs performance to each other if different metrics have been used. In a review of the performance assessment for medical BCI systems, [30] shows that the most used metrics are accuracy, accuracy combined with information transfer rate (ITR), and ITR alone. ITR is a measure that estimate the quantity of useful information transferred from brain to machine, in terms of bits per second (b/s). ITR computation takes into account the number of possible inputs, the accuracy and the latency of the system. Such metric is generic and suitable for any BCI with a finite set of inputs (e.g. speller), but is not applicable for example in BCIs using sensorymotor rhythms to move a cursor on a screen. It is also understandable that in medical BCI applications the focus is on the sole accuracy, since users do not have any other mean of communication. On the contrary, in non-medical BCI applications the latency (i.e. the time needed by the machine to detect which input the user is trying to activate) plays a critical role for the system's acceptance by able-bodied users.

In this work, the goal is to explore the capabilities and to assess the performance of plug-and-play portable BCI systems for non-medical scenarios. Therefore, the focus will be on embedded wearable non-invasive systems adopting VEPs as control signals (in particular SSVEPs), and ITR as metric for performance assessment.

2.2 EEG signal

2.2.1 Signal Description

EEG measures the electric brain activity caused by electric currents that flow within the neurons of the brain. Neurons are the cells that constitute the brain tissues and their structure is depicted in Fig. 2.1. Despite the apparent simplicity of the neural cell structure, the biophysics of neural current flow relies on complex models of ionic current generation and conduction. Basically, when a neuron is excited by other neurons through burst of action potentials (APs), excitatory postsynaptic potentials (EPSPs) are

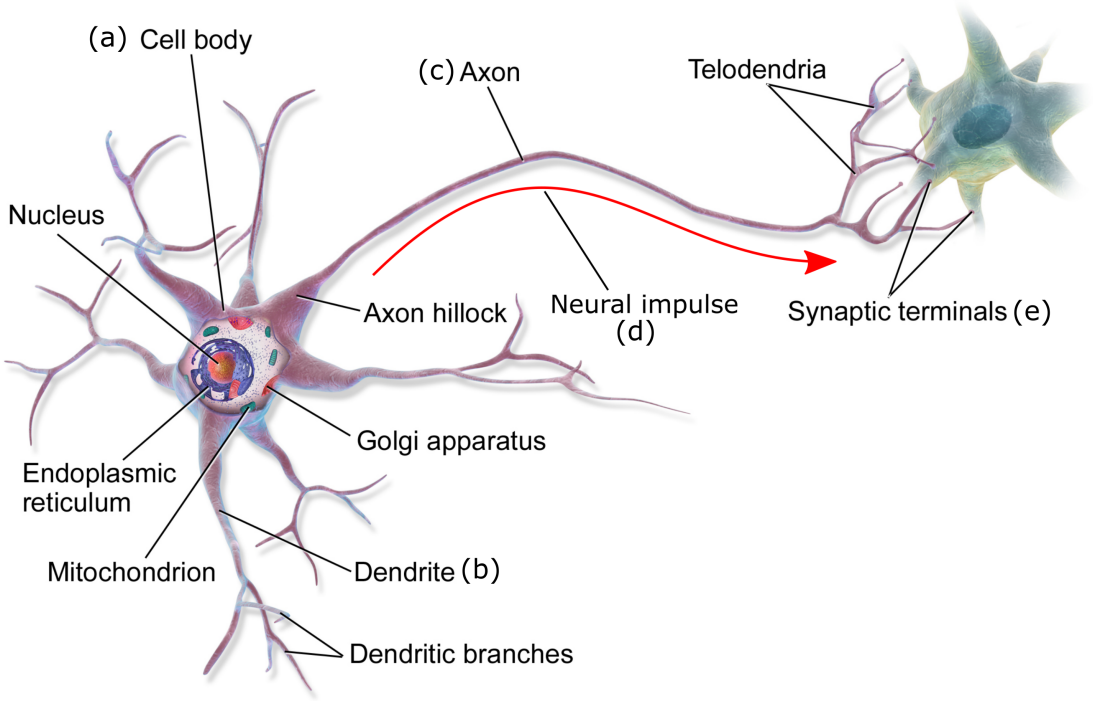

Figure 2.1: Structure of a neuron (source: Wikimedia commons). The cell body (a) contains the cell nucleus and acts as the cell's life support center. The cell body gathers and aggregates the signals arriving from other cells though dendrites (b). The axon (c) allows the neuron to spread the signal away from the cell body to other neurons. The information is constituted by a neural impulse (d), flowing from the cell body to the peripheral synaptic terminals (e), that in turn communicate with another neuron.

generated at its aptic dendritic branches. The dendritic membrane becomes depolarized and extracellularly electronegative with respect to the cell body. This potential difference causes a current, called primary current, to flow from the nonexcited membrane of the body to the dendritic tree sustaining the EPSPs [31]. The principle of conservation of electric charges imposes that the flow is looped with extracellular currents, called secondary current. Primary and secondary current both contribute to generate the magnetic field measured by the electrodes on the scalp; however, the spatial cell arrangement is critical for the superposition neural currents in order to produce measurable fields. In fact, the measured EEG signal is the result of the current generated by the EPSPs of thousands of synchronously activated neurons, because of the coherent distribution of their large dendritic trunks locally oriented in parallel, and pointing perpendicularly to the cortical surface [31]. The signal must cross several layer before reaching the electrodes places on the scalp, especially the skull, which attenuates the signal approximately one hundred times more than the soft layers [32]. Noise within the brain and over the scalp contribute to lower the SNR, and therefore only large amount of active neurons can generate enough potential to be recorded by scalp electrodes [32].

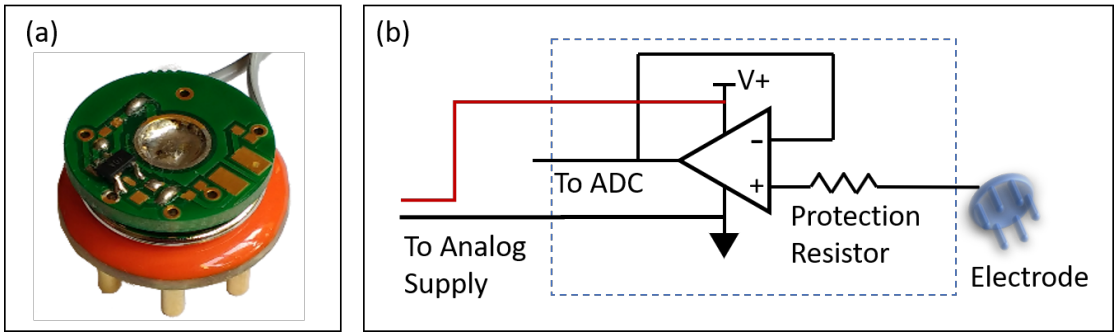

Figure 2.2: (a) Picture of the g.SAHARA dry electrode with custom amplifier PCB. (b) Electrical schematics of the custom amplifier PCB.

2.2.2 Signal Acquisition

EEG signal acquisition is an easy and non-invasive operation that allowed great spread of this technique over others (MEG, fMRI, ECoG). In fact, to acquire EEG signal it is sufficient to measure a set of electric potential differences between pairs of electrodes attached on the skin. However, detecting EEG activity is not a trivial task, since sensors and circuitry must cope with non-stable skin-electrode interface as well as with an intrinsically high-noise signal. Apart from brain activity unrelated to the SSVEP, additional sources of noise can come from acquisition system like electrical noise and external interference. The most common source of EEG signal degradation is the finite contact impedance at the interface between the electrode and the skin. A high value of contact impedance leads to a potential divider effect at the amplifier input, which causes a reduction of the capability to reject common-mode noise such as that from mains, increases the noise generated at the metal-skin interface and augments the effect of interference coupling through capacitive effects to the cables, or artifacts due to cable movement, microphony and piezoelectric effect. Contact impedance is minimized in clinical EEG protocols by removing superficial skin layers by abrasion and inserting a conductive gel or paste in-between the two surfaces. Skin preparation is obviously not suitable for non-clinical settings where system setup needs to be as quick and easy as possible for an untrained person, and associated infection risks are not acceptable.

To minimize setup time and allow self-positioning of the system, zero-preparation electrodes were adopted as interface between the system and the subject. Two options were evaluated, dry and wet electrodes. Dry electrodes are recognized as the best option for zero-preparation time. However, they present contact impedance up to 3 orders of magnitude higher than wet electrodes with skin preparation; hence, to mitigate such high contact impedance, an amplification stage is placed directly right on the electrode.

Fig. 2.2 (a) and (b) show, respectively, a picture and the schematic of the active sensor custom PCB designed for this work. As single-ended amplification stages with gain higher than one reduce the rejection of common mode noise, only signal buffering

is performed on the active electrode by a low-power, low-noise, rail-to-rail Operational Amplifier (O.A.) connected as a unity-gain buffer. Protection resistors with 68 KΩ are used to limit patient auxiliary current in cases of single fault condition below the applicable limit of 50 μA. The O.A. is an AD8603 from Analog Devices, which has a quiescent current of 50 μA and low voltage noise (2.3 μV peak-to-peak in the 0.1 to 10 Hz band and 25 nV/$\sqrt{Hz}$ at 1 KHz). The input leakage current is below 1 pA at room temperature, while total input capacitance is below 5 pF, which translates into an input impedance in excess of 500 MΩ in the EEG band. In Sec. 2.7.2, the system performance is evaluated either with wet passive electrodes (Kendall from Covidien-Medtronic [33]) and dry active electrodes (g.SAHARA from g.tec Gmbh [34]).

2.3 Taxonomy

State of the art of BCIs includes heterogeneous systems, that differ for target audience, application and design choices. A taxonomy of the existing BCIs could help to understand which kinds of devices have been developed so far. Traditionally, BCIs feature three main characteristics: independent vs dependent, invasive vs non-invasive, exogenous vs endogenous [1]. An independent BCI is a system that does not depend on peripheral nerves or muscles, which means that the brain activity necessary for controlling the BCI does not need the activity from such brain peripherals (in this case, the optic nerve is considered brain core). Examples of independent BCIs are all P300-based BCIs where the stimuli are presented one at a time. In this case, the user gaze is fixed at the single stimulus source, and the user intention is what actually triggers the BCI. Independent BCIs are often used in medical scenarios, because they are especially suitable for people suffering from severe neuromuscolar disabilities. In contrast to independent BCIs, dependent BCIs need the activity of brain's peripherals for the brain to generate the required activity. Examples of dependent BCIs are P300-based BCIs where symbols are displayed in a matrix fashion, or SSVEP-based BCIs, where all the symbols must appear to the user at the same time. In these cases in fact, it is the user's gaze that determines the required brain activity. Dependent BCIs can also be used by disabled people to some extent. For example, the aforementioned dependent BCIs can be used by people affected by Amyotrophic lateral sclerosis (ASL), as long as they can move their eyes. However, dependent BCIs are overall more suitable for able-bodied users.

Invasive BCIs are those systems that require implanting electrodes into the users' brain. This practice requires brain surgery and may affect patients' health, and it is performed for research purpose only in medical scenarios. The technique used for invasive BCIs is called electrocortography (ECoG), also known as Intracranial EEG (IEEG) [1]. ECoG allows for better SNR and better spatial resolution than EEG; however, due to

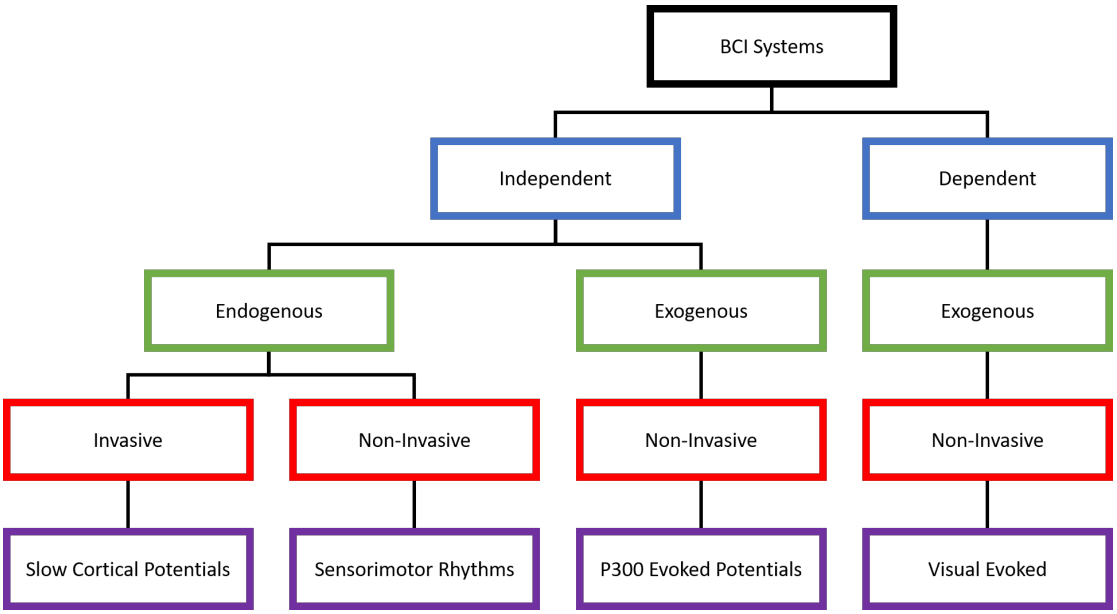

Figure 2.3: BCI taxonomy proposed by [1]. The work proposed in this thesis belongs to the Visual Evoked category: the aim is to design a dependent, exogenous and non-invasive BCI.

its unpractical and risky application this technique is not likely to spread outside clinics and research field in a near future. Non-invasive BCI systems use electrodes placed on the scalp to acquire the EEG signal, resulting in more convenient, safe and inexpensive application. Electrodes are typically placed on a wearable cap or headband, and can be easily put on and off. Wet electrodes need some skin preparation beforehand that can take up to one hour according to the number of electrodes in use. On the contrary, dry electrodes can be put on in a plug-and-play fashion, with no skin preparation, reducing the setup time to a matter of seconds.

Exogenous BCIs are those that systems exploit external stimuli in order to evoke the brain activity necessary for interaction with the machine. Examples of exogenous BCIs are those based on P300 and SSVEP potentials, and they are more suitable for plug-and-play systems since they do not require any user training. Endogenous BCIs do not rely on external stimuli, and the BCI control signals are based mainly on brain rhythms and other potential. Endogenous systems allow to interact with the BCI in a more natural manner, through user's intent. However, the user must learn to produce the specific patters that are decoded by the system, and the patterns can be meaningless encoding of BCI actions. For example, in a sensorymotor BCI the intent of moving the left arm can be mapped into a command for a household appliance. User training for endogenous BCIs is done via neurofeedback display, where the user can see how the BCI input changes according to his/her brain activity, and therefore learn how to control it. The length of the training depends on the subject, the application and the training strategy. Figure 2.3 shows the high level taxonomy proposed in [1]. One of the goals

of this thesis is the assessment of wearable, low power, fast, plug-and-play BCI systems that can be used daily in non-medical scenarios, and therefore, in the reminder of this chapter, the focus will be on dependent, exogenous and non-invasive systems based on SSVEPs.

2.4 State of the Art

Table 2.1: Comparison between state-of-the-art BCI Systems in terms of setups and ITR.

Ref.	Stimulus type	Phase synch.	Signal proc.	Synch/ Asynch	Acq. system	Training	Electrodes type	N Electrodes	Processing platform	Classifier	ITR
[35]	SSVEP	yes	TRCA	synch	Synamps2	yes	wet	9	PC	n/a	5.42
[36]	SSVEP	yes	CCA	synch	Synamps2	yes	wet	9	PC	n/a	4.50
[37]	SSVEP	no	CCA	synch	Synamps2	no	wet	9	PC	n/a	1.75
[38]	SSVEP	no	MFD	synch	Quickamp	no	n/a	1	PC	max	0.83
[39]	c-VEP	yes	CCA	synch	g.USBamp	yes	dry	16	PC	threshold	0.76
[40]	SSVEP	no	CCA	asynch	custom	no	wet	up to 16	PC	confidence indicator	0.72
[41]	SSVEP	no	PCA	asynch	g.tec	no	wet	6	PC	threshold	0.63
[42]	SSVEP	no	FFT	synch	NeuroSky	n/a	n/a	2	tablet	max	0.56
[43]	SSVEP	no	PSDA	synch	custom	no	wet	2	PC	max	0.46
[44]	SSVEP	no	FFT	synch	Blackrock Cerebus	no	dry	1	PC	threshold	0.44
[45]	SSVEP	no	PSDA CCA	synch	custom	no	wet dry noncontact	3	phone	max	0.40 0.44 0.24
[46]	**SSVEP**	**no**	**CCA**	**asynch**	**custom**	**no**	**dry**	**3**	**wearable**	**threshold**	**1.06**

After a brief story of BCIs development, this section reviews the current state of the art on BCIs focusing on dependent, exogenous, non-invasive systems, based on SSVEPs or more generally VEPs potentials. Table 2.1 shows a comparison of such systems in terms of setup and ITR.

The first BCI spellers were introduced at the end of the 80s and exploited a cerebral reaction called Event-Related Potential (ERP), consisting in very small responses to specific events or sensory stimuli, which can be detected by acquiring and processing the EEG signal on the scalp of the subject [47]. In particular, P300 is an ERP, which is elicited by a relevant stimuli (i.e. the flashing of the intended symbol), which is infrequently presented among non-relevant ones (i.e. the other available symbols). In [48], researchers presented a BCI capable of detecting 36 different target stimuli associated with the letters of the alphabet and some symbols. By repeatedly flashing entire rows or columns of a matrix constructed with the target characters, the authors capture the attended symbol as the intersection of the row and column that elicited the P300 response. This first approach to P300 BCI led to an overall performance of 2.3 characters per minute with 95% accuracy, which translates to an ITR of 0.17 bits per second.

Similar attempts were introduced later by [49] and [50], where the original Farwell

and Donchin's system is enhanced with regard to the computing platform or the processing algorithm, resulting in ITR improvements up to respectively 0.45 and 0.40 b/s. While less than half bit per second might be an acceptable transfer rate for disabled people, it is still quite a slow communication speed to be tolerated by able-bodied subjects, which most likely will refuse to adopt such system. Steady State Visual Evoked Potential (SSVEP) is another BCI paradigm that has been used in more recent works with considerable success [35–38]. This potential is elicited in the primary visual cortex as a result of repetitive external visual stimulation, and is therefore phase and frequency locked with it. Processing requires identifying the frequency (and possibly the phase) of the SSVEP signal to determine which stimuli evoked it. The SSVEP paradigm is attractive due to its higher signal-to-noise ratio (SNR) in comparison with ERPs, being significantly more immune to eye-related and electrode shifting artifacts when a proper frequency band is used [29].

SSVEPs relying only on frequency information have two major advantages with respect to mixed phase/frequency SSVEP and ERPs. The first one is that they do not require synchronization between stimuli and detection platform. This allows to minimize setup time since it considers stimulation and acquisition/processing as stand-alone systems. Such solution simplifies SSVEP use in IoT environments where the user might need to interact with several different stimuli presentation systems, which might not be on the same network or might not be connected at all [51]. The second advantage is that they can operate directly without the need for a training phase in which the BCI adapts to the specific user. As this training is often a function of the specific session setup (including exact electrode position and contact quality), in many cases it must be periodically repeated [52], severely hampering the plug-and-play features of such a device. Nevertheless, many works still rely on both frequency and phase, significantly reducing the advantages of such techniques and focusing only on maximizing ITR [53]. This work demonstrates that practical ITR can be achieved with "frequency only" SSVEP [46].

Basic feature extraction for SSVEP can be performed using simple techniques. An early example is found in [54], where the authors designed and implemented a BCI to help users to input phone numbers based almost entirely on FFT-based Power Spectral Density Analysis (PSDA). Some studies later combined FFT-based features with more advanced classification algorithms such as Linear Discriminant Analysis (LDA) [55], Support Vector Machine (SVM) or Artificial Neural Networks (ANNs) [56] to improve performance. Nevertheless, these systems are relatively slow, with ITR of 0.56 and 0.44 b/s, respectively.

Other systems employ different signal processing techniques like PSDA [43, 45], PCA [41] and Matched Filter Detector (MFD) [38]. Chi et al. [45] and Garcia et al. [43] developed a BCI based on custom acquisition systems. The former uses LED matrices for stimuli presentation, while the latter focuses on assessing the performance of three

types of electrodes: wet, dry and contactless. Both of them use PSDA for features extraction, achieving an ITR of respectively 0.44 and 0.46 b/s. Cecotti [41] proposes an asynchronous multilevel speller grouping letters within three stimuli, meaning that for each letter selection the BCI must correctly perform SSVEP detection three times. Feature extraction is performed using PCA, and the ITR is 0.63 b/s. Chang et al. [38] analyzed SSVEP response with a MFD, which consists of a bank of matched filters, followed by an amplitude detector. The authors managed to remotely control a wheel robot, achieving an ITR of 0.83 b/s using only one electrode.

Such systems have the common drawback of low ITR. To tackle this issue, a well accepted solution is represented by the use of Canonical Correlation Analysis (CCA). Developed by Hotelling [57] and first introduced by Lin et al. in the BCI context, it explores the relationship of two multivariate sets of variables, determining if they have some underlying correlation [58]. Lin et al. [58] employed CCA to extract the correlation features from nine frequency-coded simulations from multiple EEG channels, demonstrating that ITR can be improved with respect to FFT-based methods. Authors in [59] have also confirmed that CCA outperforms FFT-based methods in accuracy and response delay. Using a joint frequency-phase modulation method to tag 40 characters with 0.5-s-long stimuli, authors in [36] have developed a noninvasive BCI capable of achieving an ITR of 4.50 b/s. Some attempts were made also with similar correlation analyses, like in Nakanishi et al. [35] where a high speed SSVEP brain speller uses Task Related Component Analysis (TRCA), a spatial filtering in which weight coefficients are optimized to maximize the covariance of time-locked SSVEP trials. The authors achieved 5.42 b/s ITR using 9 channels and 40 phase-locked flickering targets. Another powerful method for direct frequency estimation, described in [60, 61], is based on the Vandermonde decomposition. Although this solution provides a direct frequency estimation with a short time window, its computational complexity hinders the implementation on a resource-constrained platform because of the large dimension ($> 64 \times 64$) of the input matrices calculated to execute the algorithm.

The approaches cited above can reach high level of ITR, enabling a fast BCI for SSVEP decoding. Anyway, they require a training session to adapt the setup on the user. A solution to adapt the CCA without specific subject-dependent training is presented in [37], where authors include in the CCA the information of frequency harmonics from 9 EEG channels, achieving an ITR of 1.75 b/s using 42 different frequency-coded stimuli. Nevertheless, all the aforementioned solutions require a synchronization mechanism between stimuli and acquisition phases. Moreover, to maximize accuracy and ITR, EEG acquisition systems rely on 9 wet electrodes, which limit ease-of-use and unobtrusiveness, hindering the deployment of such solutions in wearable, minimally invasive form-factor.

The work presented in [40] represents a step forward in the development of a CCA

based system, since it is based on non-synchronized stimuli presentation and it does not require subject-dependent training. However, it achieve an ITR lower than 1 b/s, with a bulky setup, based on 16 wet EEG electrodes.

The lesson learned from the analysis of the SoA in BCI speller is that the development of a high-performance wearable platform for BCI spelling is still an open challenge. Although some systems target a portable setup, (e.g. a tablet [42] or a smartphone [45]), they achieve low values of ITR, in a bulky setup (i.e. many electrodes which requires skin preparation) with power-hungry computational platforms.

Hence, the goal of this chapter is to show a design for a wearable BCI system that relies on a minimally intrusive setup (i.e. 3 dry sensors), without subject dependent training and stimuli synchronization, and achieving ITR higher than 1 b/s.

2.5 Canonical Correlation Analysis

The state-of-the-art algorithm for SSVEPs detection is named Canonical Correlation Analysis (CCA) [62]. This method quantifies the linear dependency between two multidimensional variables by finding a couple of linear combinations, one for each multidimensional variable, that maximizes their correlation. The resulting maximized correlation is called canonical coefficient and extends the concept of correlation to multidimensional variables. More than that, CCA actually provides a whole set of canonical coefficients, sorted by size. The first canonical coefficient of the set is the biggest, and represents the correlation between a pair of linear combinations that maximizes the correlation. The second canonical correlation coefficient is the second biggest, and represents the correlation between another pair of linear combinations, that are uncorrelated with the previous pair. The number of canonical correlation coefficients and corresponding linear combination pairs depends on the dimension of the two variables, and corresponds to the minimum of the dimension of the two variables. In SSVEP-based BCIs, the two multidimensional variables to be correlated are the n EEG input channels, and a set of m reference signals that identify the frequency of one single stimulus, usually sine and cosine of that frequency and one or more harmonics. Therefore, one execution of the CCA algorithm returns a set of size $d = min(n, m)$ of canonical correlation coefficients that quantify the correlation between the EEG signal window and one specific stimulus. In order for the system to compute an output, it is necessary to retrieve canonical correlation values with respect to all the reference signal sets, which means executing CCA for each possible stimulus. Figure 2.4 summarizes the CCA algorithm and its actual implementation on many statistical packages.

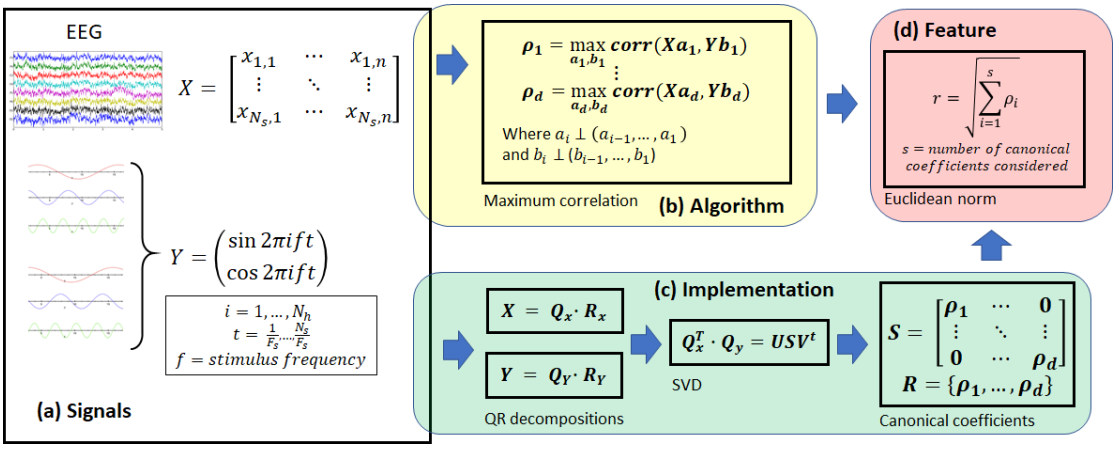

Figure 2.4: Block diagram of CCA algorithm and implementation. (a) Signal matrices input for CCA. (b) CCA formulation algorithm. (c) CCA implementation algorithm. (d) Feature extraction.

Formally, let us define the multidimensional variable X as a time window of length N_s samples of the n EEG input channels, such that:

$$X = \{X_1, X_2, ..., X_n\},$$

$$X_i = \{x_{i,1}, x_{i,2}, ..., x_{i,N_s}\},$$

$$i = 1, \dots, n.$$

Let us define the reference signals as a set of sine and cosine of the stimulus frequency f and its N_h harmonics, then the multidimensional variable Y is defined as follows:

$$Y = \begin{pmatrix} Y_1 \\ Y_2 \\ Y_3 \\ Y_4 \\ \vdots \\ Y_{m-1} \\ Y_m \end{pmatrix} = \begin{pmatrix} sin(2\pi ft) \\ cos(2\pi ft) \\ sin(4\pi ft) \\ cos(4\pi ft) \\ \vdots \\ sin(2N_h\pi ft) \\ cos(2N_h\pi ft) \end{pmatrix}$$

$$\text{for } t = \frac{1}{F_s}, \frac{2}{F_s}, \cdots, \frac{N_s}{F_s}$$

where F_s is the sample frequency of the EEG acquisition system. Let us define the linear combinations of X and Y as:

$$U = Xa$$

$$V = Yb$$

Then the function to maximize is:

$$\rho = \max_{a,b} corr(Xa, Yb)$$

After retrieving the first canonical correlation coefficient ρ_1 and the corresponding couple of linear combination coefficient matrices a_1 and b_1, the algorithm continues the search looking for a couple (a_2, b_2) such that the linear combinations $U_2 = Xa_2$ and $V_2 = Yb_2$ belong to an orthogonal subspace with reference to $U_1 = Xa_1$ and $V_1 = Yb_1$. The search continues until the orthogonal subspaces of the less ranked multidimensional variable are exhausted, resulting in a vector of canonical coefficients

$$R = \{\rho_1, \rho_2, \ldots, \rho_d\}$$

sorted in decreasing order. Quite often only the first canonical coefficient is used as feature for frequency detection. However, authors in [63] proved that the combination of the information held by the other coefficients helps to improve frequency detection accuracy. In particular, the feature used for frequency detection is calculated as the Euclidean norm of the first s canonical coefficient:

$$r = \sqrt{\sum_{i=1}^{s} \rho_i}$$

In this work, the Euclidean norm of the first $s = 3$ canonical coefficients is used as a feature for frequency detection. The implemented algorithm is described later in Sec. 2.6.2

2.6 Wearable BCI

The system presented is a novel embedded asynchronous BCI featuring a custom acquisition platform and non-invasive dry electrodes for real-time classification of eight frequency-coded stimuli. Being able to operate in stand-alone mode, it provides full portability by removing the need for any external processing device. At the core of the system, a CCA-based algorithm performs the feature extraction of the incoming EEG signals from three dry electrodes. The system requires no training phase and does not need to tailor any parameter on the specific subject or trial, as all critical parameters of the system, such as the number of channels and location, frequency band, and window

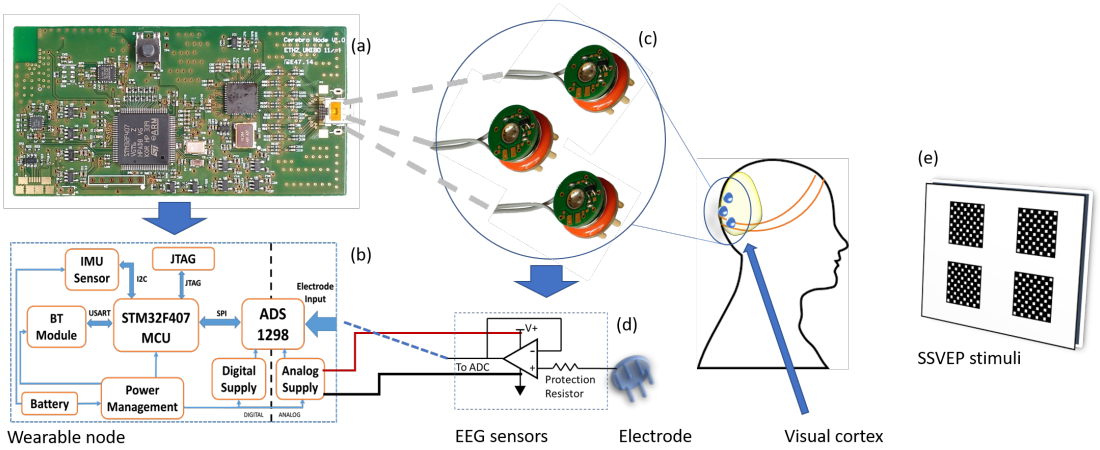

Figure 2.5: Architectural diagram of the proposed system. Fig. 2.5 (a) and (b) show, respectively, an image and the block diagram of the wearable node. Fig. 2.5 (c) presents an image of the dry active electrodes and (d) the electrical schematics of the custom amplifier stage PCB. Finally, in Fig. 2.5 (e) the LCD screen with stimuli presentation is depicted.

lengths, are fixed through offline data analysis before the final implementation in a user-independent fashion. An overview of the overall system is depicted in Fig. 2.5.

The wearable platform is designed for medical IoT applications and derived from [64] and [65]. The system is composed of an active EEG sensor array interfaced to a custom board with a biopotential ADC and a low power microcontroller with DSP capabilities. It acquires and processes the subject response to a visual stimuli. The results of the CCA analysis, computed in real-time on the microcontroller, can then be communicated to the host PC as HMI commands.

2.6.1 Hardware

The proposed IoT node is based on a multichannel commercial Analog Front End (AFE) [66] connected with a low power ARM Cortex M4 microcontroller. The AFE is the *de-facto* standard used in biopotential acquisition platforms. The 8 channels are connected in single ended configuration with the active EEG sensors while the AFE's back-end streams the data via SPI to the microcontroller. The ARM Cortex M4 microcontroller is equipped with a single precision FPU unit and has an instruction set architecture with DSP extensions to enable a more efficient near-sensor processing. It can reach operating frequency of 168 MHz with 192 kB of RAM and 1 Mb of FLASH memory.

The board is a 6-layers Printed Circuit Board (PCB) with a single solid ground plane. To minimize current return paths, the power planes are split, keeping separated the analog and digital circuitry. Discrete components were carefully placed on both sides of the PCB to maximize signal integrity, maintaining a low level of noise and a small

form-factor that results in 85x50 mm. The board mounts a dedicated IC for power management, that automatically detects the power source (battery or USB). Analog, digital and communication subsystems are supplied by separate low-dropout voltage regulators. This versatile configuration allows power management strategies, like duty-cycling submodules, to enhance battery life.

2.6.2 Firmware implementation

All firmware has been implemented in C language on a low-power ARM CORTEX M4 microcontroller, using *STM32 WorkBench*, a dedicated Integrated Development Environment (IDE) based on the open-source GCC compiler version 5.4.1. The proposed implementation of CCA is based on the Golub algorithm [67, 68], which, by virtue of its computational efficiency, is widely used in many statistical packages [69]. The Golub algorithm relies on the computation of two QR decompositions, followed by a SVD factorization. The implemented algorithm is summarized in Fig. 2.4c.

In the implementation of the firmware, this algorithm must be executed N_f times, once for every stimulus presented at different frequency, and its execution must be optimized in order to achieve near real-time performance even with several stimuli. Three levels of optimization are applied: (i) usage of CMSIS-DSP library provided by ARM whenever possible [70], (ii) precomputation and storage in Flash memory of the orthogonal matrices Q_y resulting from the QR decomposition of all the reference signals, and (iii) input filtering and downsampling. A time window of the acquired EEG signal channels constitutes the multidimensional variable X. The length N_s of the time window is a parameter affecting the overall BCI performance, and its computation is described later.

Before applying CCA, the input signal must be preprocessed in two steps: (i) a band pass filter is applied for removing low frequency and 50 Hz noise, and allowing a downsampling factor up to 10, that reflects in a speedup > 4 in CCA computation; (ii) all the channels are reduced to zero mean in order to be later correlated with the reference signals. The band pass filter features a low pass 100 taps FIR with cutoff frequency at 18.4 Hz, and a second order high pass IIR. The low pass FIR filter guarantees to preserve the signal amplitude up to the first harmonic of the higher stimulus frequency, since this system uses $N_h = 1$, and at the same time it achieves 60 dB attenuation at 50 Hz, without introducing excessive delay or computational effort.

After preprocessing, the resulting multidimensional variable X must be correlated with the corresponding reference signals for each frequency used for the stimuli. The QR decomposition is therefore computed once only, obtaining the orthogonal matrix Q_x, then the algorithm enters a loop for each stimulus frequency k, where the same Q_x

matrix is multiplied by the corresponding $Q_y(k)$ matrix already precomputed and stored in Flash memory. The resulting matrix is factorized by the SVD, where the optimized code skips all the computation that involves elements of the matrices which zeros values.

All the coefficients of the diagonal matrix S obtained by the decomposition are used in the computation of the Euclidean norm, which is the measure of the correlation between EEG and reference signal that is used for frequency detection. The algorithm performance is discussed in Sec. 2.7.3.

Since this BCI system is asynchronous, independent and potentially disconnected from the source of the stimuli, at the end of each data window processing the system must deliver some output, regardless of actual activity of the user. The frequency classification is performed by simple thresholding: if the maximum of the N_f correlation features exceeds the threshold, then the BCI output is the corresponding frequency, otherwise the system output is the rest or idle state, decoded with class 0. The choice of the threshold value will be discussed in Sec. 2.7.2.

2.7 Experiments and results

2.7.1 Experimental setup

A graphical interface of the SSVEP-based BCI system usually consists of different areas of a screen which are associated to different commands, e.g. letters or symbols, that flicker at specific frequencies. When the user pays attention to a particular flickering command, SSVEPs are induced at the corresponding frequency and its harmonics. The BCI system identifies the user intention by quantifying and classifying SSVEP. It is generally acknowledged that the SSVEP response depends on the frequency of the stimulation, nevertheless there is no consensus on which frequency bands are better suited for maximizing information transfer rate and accuracy. Regan has shown three distinct maxima in the response to flickering stimuli at 10, 13-25 and 40-60 Hz [71]. Other subsequent works showed similar results [72]. Kuś et al. [73] observed how signal-to-noise ratio of SSVEP signal vs. unrelated brain activity is maximized in the 8-20 Hz band, however not taking into account higher order harmonics in the computation. It should be observed that, in general, the lower the target frequencies, the lower the sampling rate required to the system, and consequently its power consumption, which is of major importance in portable systems.

The BCI system presented in this work is the product of an initial phase of offline tests used to fix critical parameters, such as the number and location of electrodes, frequency intervals, window length for data processing, etc. Subsequently, online tests have been carried out to assess the real-time performance. Eight healthy subjects (aged 25-40

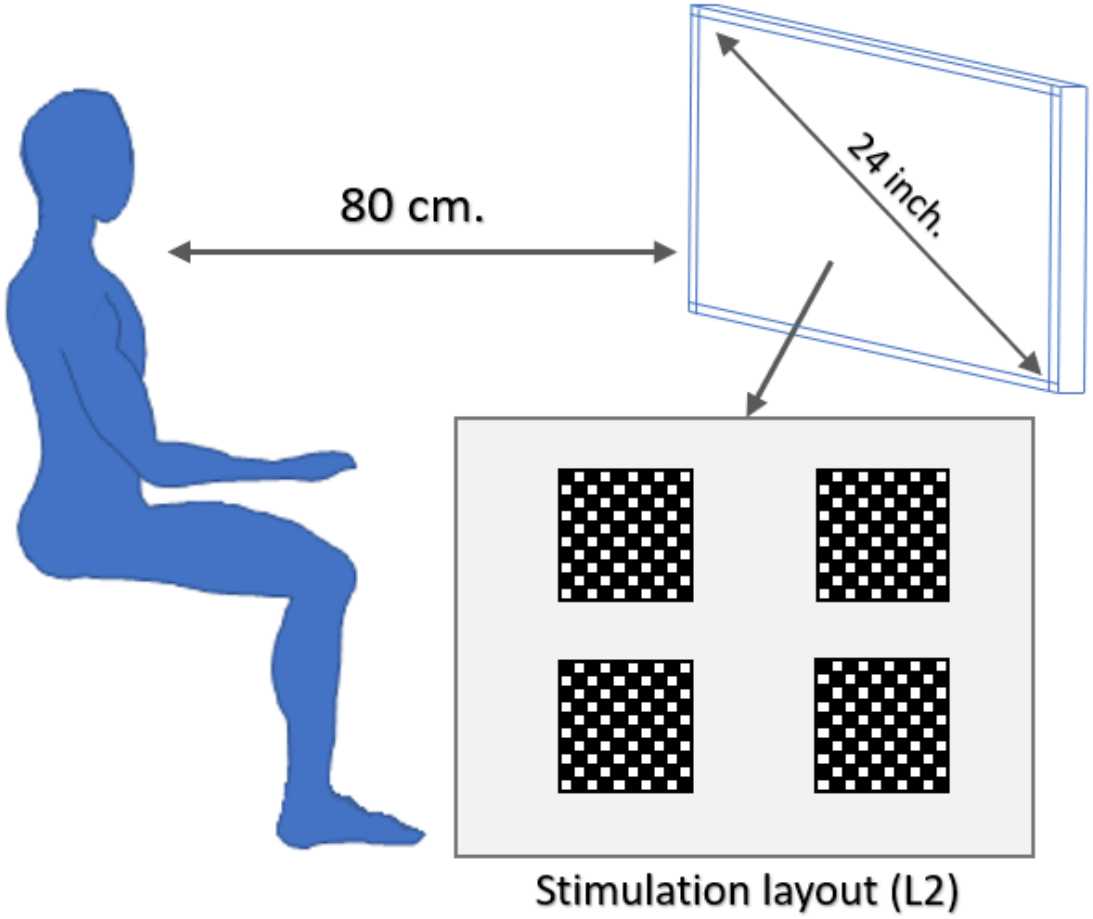

Figure 2.6: Acquisition setup: the flickering stimuli layouts (layout L2 in the figure, featuring four checkerboards) are presented on a 24-inches LED screen. The subject stares at the screen from a distance of 80 cm.

years) with normal or corrected-to-normal vision participated in the offline experiments. Another group of five subjects was taken later for the online tests. All participants reported no history of neurological or psychiatric disorders and provided a written consent to participate in the experiments.

SSVEP signals are elicited by adjusting the luminosity (contrast) of black and white 10 x 10 square checkerboards [74] on a grey background employing the sampled sinusoidal stimulation method [75] on three different layouts. The first layout (L1) only contains one checkerboard covering 75 % of the screen and centered at the middle point and is employed to display different stimuli in successive order. The second layout (L2), comprises four checkerboards arranged in a 2 x 2 pattern at equidistant positions, each displaying a different frequency-coded stimulus (a single checkerboard occupies 20 % of the screen). The third layout (L3) contains eight checkerboards arranged in a 2 x 4 pattern, each one covering 10 % of the screen. The design of the layouts aims to test the level of response of the SSVEP signals with consecutive smaller stimuli in the presence of non-target stimuli. Fig. 2.6 depicts the acquisition setup with L2.

The luminosity (contrast) of the checkerboards was adjusted using the following equation:

$$Contrast(f, \phi, i) = A \cdot sin(2\pi fi/F_r + \phi) + A$$

where i indicates the frame index, A the initial amplitude, ϕ the initial phase, constant for all experiments (ϕ=0), f the frequency of the stimulation, and F_r is the refresh rate of the screen. All checkerboards included a grey diagonal cross to help visual fixation. All the textures were generated using Psychtoolbox 3.0.10 for Windows in Matlab 9.1. All the layouts were presented on a 24-inch LED (60fps) screen at a distance of approximately 80 cm. This setup is fixed for all the subjects, in order to measure the SSVEP elicited by the most uniform stimulation possible. Since there is no uniformity in literature for the distance between the subject and the screen ([3, 76, 77]), this choice is arbitrary.

EEG data were acquired using the hardware presented in section 2.6.1 at a sample rate of 1 KHz. For the offline test, five electrodes over the occipital lobe (P5, PO3, POZ, PO4, and P6) and two over the frontal lobe (F3 and F4) were placed to record the SSVEPs, with reference and ground electrodes located at A1 and A2 respectively. Online tests were performed only with three electrodes, located at P5, POZ, and P6, while reference and ground remained at the same position. Electrodes impedance was kept below $10K\Omega$. Triggers generated by the stimulation program were bound to the incoming raw data by custom software. It is worth mentioning that all experiments were repeated twice to evaluate the performance of the dry electrode system with respect to a classic wet configuration.

Equally spaced frequency-coded stimuli ranging from 5 Hz to 17.5 Hz, with a step of 1.2 Hz were used to select suitable frequency targets. Each trial included five seconds of stimulation followed by 5 seconds of pause to reduce visual fatigue. The results from eight test subjects are summarized in Fig. 2.7 showing that the range of frequencies between *5-12.2 Hz* have a significantly higher average correlation magnitude. Nevertheless, the useful range has been narrowed up to 9.5 Hz to avoid any interference from the alpha band in the final implementation. Simultaneously, the design exploits an exhaustive search to determine the minimum number of electrodes required, finding that there are no significant differences in correlation when using only the electrodes P5, POz and P6 with respect to the full setup. Thus, the final system adopted these changes allowing us to maximize the performance while reducing overall the complexity and intrusiveness of the hardware. It is worth noticing that Fig. 2.7 only presents the results of the wet-electrodes test since there are no significant differences when using dry electrodes.

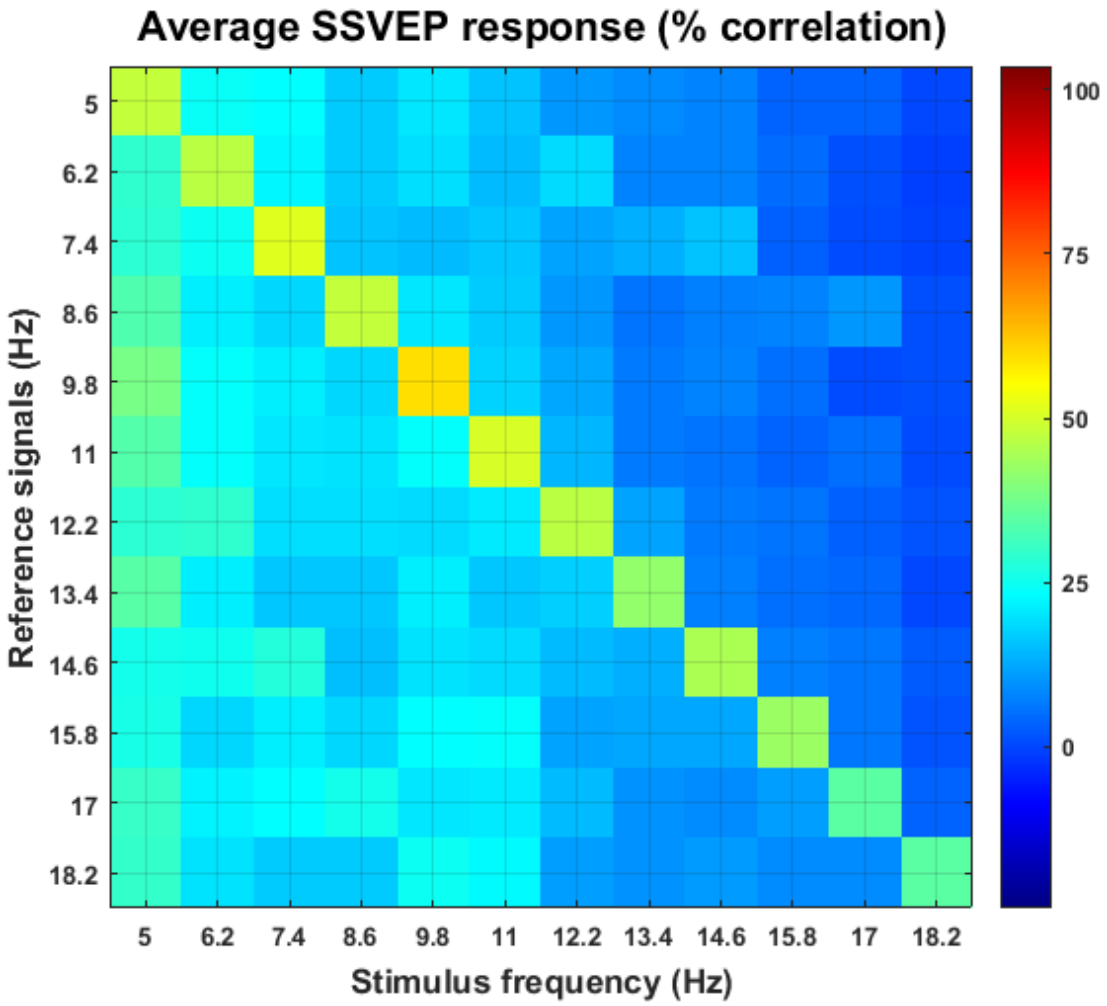

Figure 2.7: Average CCA correlation of SSVEP responses for different stimuli (x-axes) calculated with different reference signals (y-axes). On the diagonal it is possible to observe higher correlation due to the correspondence between the stimulus frequency and the reference signals. Noticeably, the lower part of the stimuli spectrum allows for higher correlation response with respect to the higher part.

2.7.2 Experimental results

The system presented at 2.6.2 was evaluated using dry and wet electrodes while performing a new test session using L2 and L3 layouts presenting four and eight simultaneous stimuli, respectively. All the stimuli were coded using a $\Delta F = range/N_{stimuli}$, to allow maximum separation between targets in the frequency range. The subjects (same as the previous test) fixed the sight at the target frequency indicated with a red square before the onset of the stimulation. Later, all the stimuli remained active for five seconds with a resting time of 5 seconds in between trials. The experiment ends when the subject has been staring once at each stimulus on the screen.

An exhaustive analysis of the offline results shows that the most performing data window length is 2 s for both wet and dry systems, which turns in $N_s = 2000$ samples

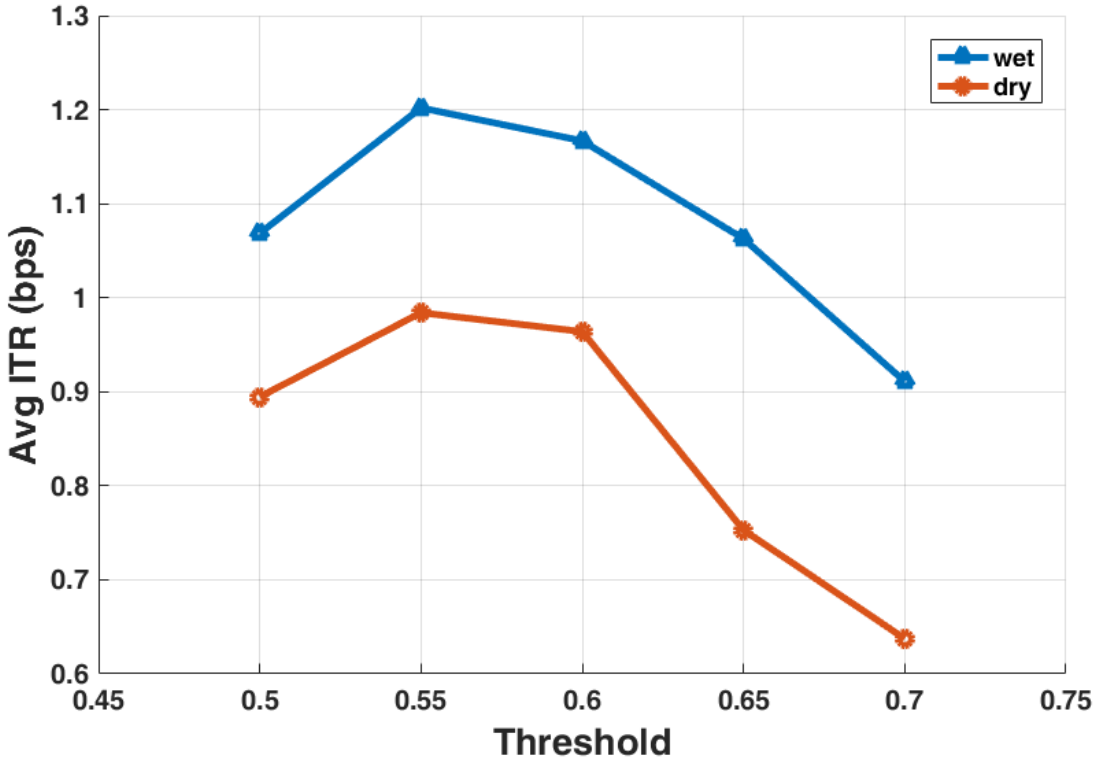

Figure 2.8: Average ITR results for the system with wet electrodes (blue triangles), and dry electrodes (red circles) calculated using different classification thresholds. A threshold value of 0.55 is shown to maximize ITR for both wet and dry electrodes.

to process for each channel at each CCA iteration. This window size guarantees a good trade-off between system latency ($\sim 2s$) and accuracy ($> 90\%$). Even if the system is asynchronous, offline system latency is assessed by measuring the time interval between the stimulus onset and the first correct detection. For detailed results description refer to tables 2.2 and 2.3. The other parameter of the system, the classification threshold, is chosen to maximize the average ITR, calculated for the asynchronous BCIs as in [78]:

$$ITR = \frac{1 - P_r}{d_{avg}} \left(\log_2 N_f + (1 - P_w) \log_2 (1 - P_w) + P_w \log_2 \left(\frac{P_W}{N_f - 1} \right) \right)$$

where P_r is the probability of non-detected stimuli or trial error, P_w is the probability of incorrect detected cases, N_f is the number of target stimuli, and d_{avg} is the average delay or latency of the system in seconds. Fig. 2.8 depicts the values of the average ITR of the wet and dry system calculated with several thresholds. The figure shows that the threshold value of 0.55 maximizes both curves, therefore it is the most suitable threshold value to use for the BCI output classification.

Tables 2.2 and 2.3 show the classification performance using four and eight stimuli

for wet and dry electrodes. Even though the average latency for the 4-stimuli wet system is smaller than the 8-stimuli system, the latter achieves higher ITR due to the increase in the number of targets. This situation improves when analyzing the dry systems, where the 8-stimuli not only outperforms the 4-stimuli, it also achieves similar performance than the wet system. These results also demonstrate that the interference created by placing different stimuli at the same layout with decreasing target size is negligible.

Following the results introduced above, the system is validated while performing the acquisition of the EEG data and classification in real time, employing five test subjects, that have not been involved in the offline experiments. To ease the computation of the results, the outputs of the classification are transmitted directly to a computer using a BT communication module, automatically synchronized with the onset of the corresponding stimulation by a custom software. During the experiments, the checkerboards with the target frequency were indicated with a red square that appears before the stimulation. Once a valid frequency was detected, the stimulation was stopped and the detected frequency was highlighted and cued with a white frame. The accuracy of the system was then asserted by the number of correct classifications over the total number of classifications, and the latency is computed as the time needed for detection of the trials that succeeded. The results of the experiment are summarized in tables 2.4 and 2.5, allowing us to conclude that there are no significant differences between offline and online experiments. Also, the average ITR using eight stimuli and the dry sensor interface is 1.25 b/s, proving that the introduced embedded implementation can achieve performance that is comparable with non-wearable systems [37–39, 41], while outperforming other wearable or mobile systems [40, 42, 45].

Table 2.2: Offline results for 4 stimuli BCI, wet and dry setup.

	Total accuracy (wet / dry)	Trial accuracy (wet / dry)	Latency [s] (wet / dry)	ITR [b/s] (wet / dry)
S1	0.97 / 0.98	1 / 1	1.91 / 1.86	0.94 / 1.00
S2	0.96 / 0.96	1 / 0.75	1.57 / 2.41	1.07 / 0.53
S3	0.98 / 0.96	1 / 1	1.60 / 1.83	1.12 / 0.91
S4	0.95 / 0.96	1 / 0.75	2.10 / 1.91	0.79 / 0.67
S5	0.96 / 0.98	1 / 1	1.41 / 1.65	1.19 / 1.11
S6	0.99 / 0.97	1 / 1	1.33 / 1.60	1.42 / 1.09
S7	0.95 / 0.99	1 / 1	0.86 / 1.17	1.90 / 1.59
S8	0.97 / 0.98	1 / 1	1.33 / 2.00	1.32 / 0.90
Average	**0.97 / 0.97**	**1 / 0.94**	**1.51 / 1.80**	**1.22 / 0.98**

Table 2.3: Offline results for 8 stimuli BCI, wet and dry setup.

	Total accuracy (wet/dry)	Trial accuracy (wet/dry)	Latency [s] (wet/dry)	ITR [b/s] (wet/dry)
S1	0.92 / 0.92	1 / 1	2.11 / 2.84	1.12 / 0.84
S2	0.93 / 0.93	1 / 1	1.43 / 1.66	1.69 / 1.48
S3	0.89 / 0.96	1 / 1	2.24 / 3.25	0.99 / 0.82
S4	0.94 / 0.92	1 / 1	1.71 / 1.87	1.46 / 1.27
S5	0.95 / 0.97	1 / 1	1.70 / 1.59	1.51 / 1.70
S6	0.98 / 0.98	0.75 / 1	2.37 / 2.17	0.90 / 1.28
S7	0.74 / 0.94	1 / 1	1.21 / 3.42	1.20 / 0.74
S8	0.92 / 0.91	1 / 1	1.53 / 1.58	1.54 / 1.48
Average	**0.91 / 0.94**	**0.97 / 1**	**1.79 / 2.30**	**1.30 / 1.20**

Table 2.4: Online results for 4 stimuli BCI, wet and dry setup.

	Total accuracy (wet/dry)	Trial accuracy (wet/dry)	Latency [s] (wet/dry)	ITR [b/s] (wet/dry)
S1	0.88 / 0.87	1 / 1	0.76 / 3.01	1.69 / 0.41
S2	0.87 / 0.91	1 / 1	0.76 / 1.34	1.64 / 1.06
S3	0.91 / 0.92	1 / 1	1.44 / 2.05	1.01 / 0.72
S4	0.93 / 0.94	1 / 1	2.16 / 1.31	0.70 / 1.24
S5	0.89 / 0.92	1 / 1	1.36 / 0.99	0.96 / 1.48
Average	**0.89 / 0.91**	**1 / 1**	**1.30 / 1.74**	**1.20 / 0.99**

Table 2.5: Online results for 8 stimuli BCI, wet and dry setup.

	Total accuracy (wet/dry)	Trial accuracy (wet/dry)	Latency [s] (wet/dry)	ITR [b/s] (wet/dry)
S1	0.83 / 0.83	1 / 1	2.01 / 2.52	0.92 / 0.74
S2	0.84 / 0.88	1 / 1	1.19 / 1.34	1.62 / 1.57
S3	0.89 / 0.86	1 / 1	1.18 / 1.50	1.83 / 1.36
S4	0.81 / 0.76	1 / 1	1.65 / 1.40	1.07 / 1.08
S5	0.79 / 0.83	1 / 1	1.79 / 2.02	0.94 / 0.92
Average	**0.83 / 0.83**	**1 / 1**	**1.56 / 1.76**	**1.27 / 1.13**

2.7.3 Computational results

The algorithm described in 2.6.2 was implemented on the board described in 2.6.1. DMA transfer, clock gating and optimization of clock frequency were used to minimize the power consumption. To speed up execution time, the code employs CMSIS [70] functions when possible, and pushed compiler optimization to -O2 within those functions. As mentioned before, the number of samples to process at each CCA iteration is 2000. However, it is possible to downsample the data up to factor 10 for a twofold goal: reduce power consumption and decrease the delay between two consecutive classifications. In fact, higher BCI output frequency contributes to boost ITR and to enhance the user real

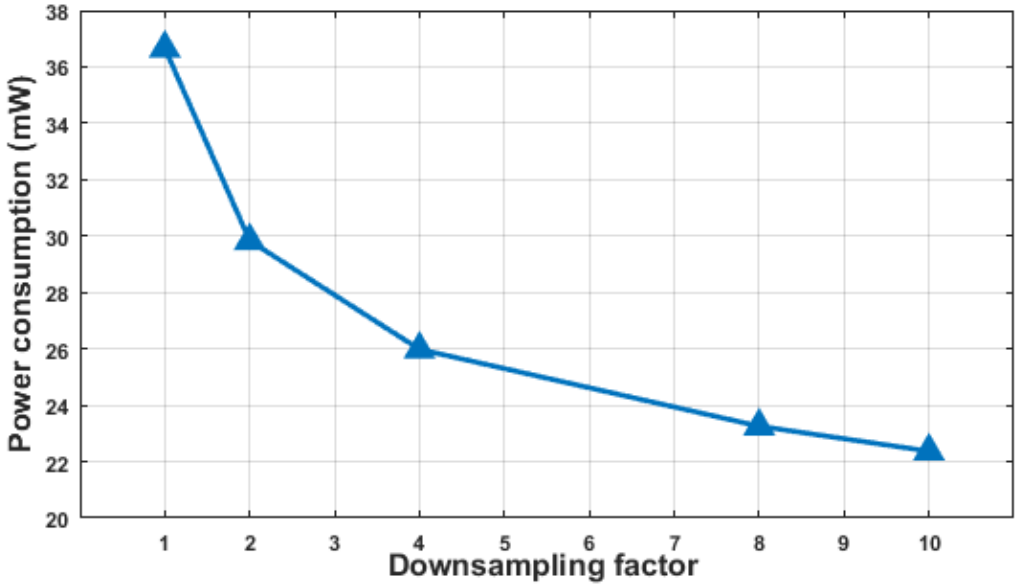

Figure 2.9: Trend of the power consumption calculated for several downsampling factors (blue triangles) for four stimuli.

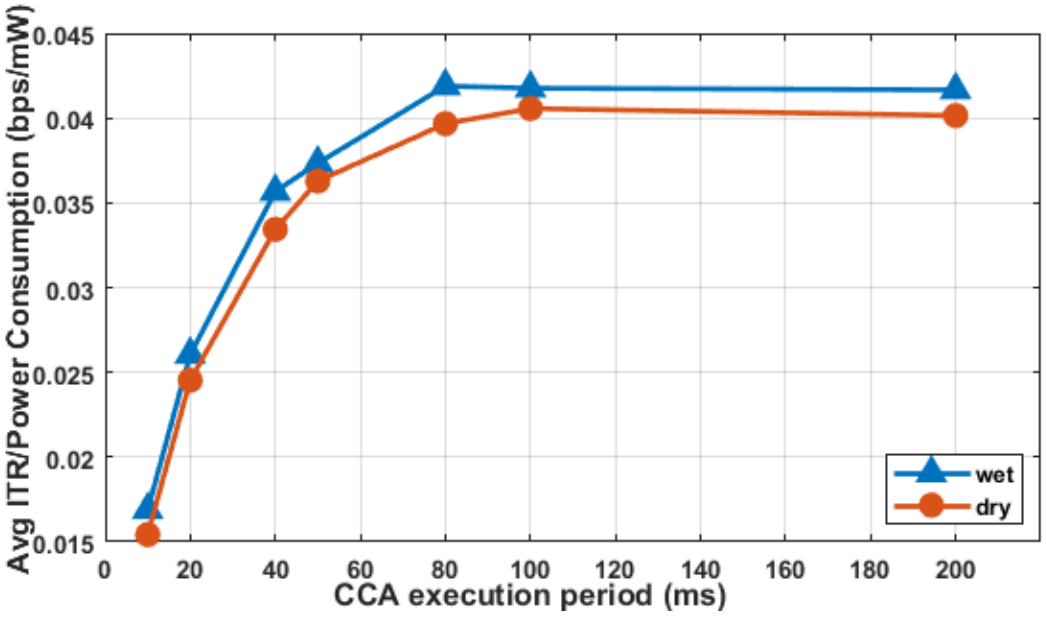

Figure 2.10: Trend of the ITR/power consumption ratio calculated for several CCA execution periods with wet electrodes (blue triangles) and dry electrodes (red circles).

time experience. Downsampling 10 allows to reduce MCU cycles from about 3157k to about 768k, achieving speedup > 4 without significantly degrading the accuracy. In fact, while ITR remains constant, Fig. 2.9 shows the decreasing curve of power consumption according to downsampling factor.

The time needed to execute the optimized algorithm on the custom device is less than 5 ms, which allows us great liberty in the choice of the performance/power consumption

trade-off. In principle, the power consumption decreases when the CCA execution period increases, because the algorithm is execute less frequently. At the same time, also the ITR decreases due to BCI response latency growth. Fig. 2.10 shows the trend of the ITR over power consumption with reference to the period of the CCA execution. The curves suggest that 100 ms is a good CCA execution period for both dry and wet systems, in fact 100 ms period guarantees average ITR $> 1b/s$, power consumption of 22.4 mW for four stimuli and 27.5 mW for eight stimuli, and ten outputs per seconds for a real-time user experience. The power consumption was measured on the board using a source measure unit instrument.

Chapter 3

Location-Based BCI

Geolocation is the enabling technique for a wide spectrum of Location-Based Services (LBS) involving, for instance, navigation, transport, tourism, entertainment, healthcare and augmented reality applications. While outdoor localization is mostly solved by Global Positioning System (GPS) technology, indoor localization is still an open issue due to heterogeneity of indoor environments and impracticality of a common approach for all single cases [79]. In fact, GPS is an unreliable technology for indoor positioning, since its signal is not strong enough to be correctly received inside buildings.

Several approaches for indoor localization have been proposed. Some of them exploit existing communication infrastructures like WiFi [80] and FM radio signals [81], others rely on ad-hoc infrastructures like ZigBee [82], Bluetooth [83], Ultra Wide Band (UWB) [84] and Radio Frequency Identification (RFID) [85]. Other systems do not need any kind of specific infrastructure, since they compute the device position using embedded sensors like magnetometer [86], accelerometer, and gyroscope. Furthermore, several hybrid approaches have been proposed, based on complementary technologies like inertial sensors and WiFi [87] or Bluetooth and WiFi [88]. Merging geolocation with EEG monitoring can serve as a tool to understand the brain activity during daily tasks, empowering the efficiency of future BCI systems in interpreting the user's intentions and functional state of mind. However, only few contributions proposed a system that combines the two information sources. In [89], the authors propose a BCI system for controlling a wheelchair, based on the P300 evoked potential and triggered though the oddball paradigm technique. The authors achieved geolocation implementing an optical-based tracking system on the wheelchair. In [90], the author proposes a cloud based solution for patients localization and monitoring in terms of voice pathology detection. In this solution, EEG signal is acquired through a deeply embedded system attached to the outer surface of the patients' vocal fold, while localization is performed via GPS and WiFi.

Differently from the aforementioned papers, the aim of this work is to create a Hardware-Software platform to bind the EEG response with the position of the subject, to understand the challenges on the acquisition of EEG signals in real environments, hindered by artifacts, external noise and hardware constrains, and to study the correlations between the brain activity and the subject's location or movements. To achieve this goal, the system proposed in Sec. 2.6 is paired with an Android application capable of tracking the subject in an indoor environment. The indoor tracking is performed by IndoorAtlas [91], a cloud based service that exploits smartphone embedded magnetometer for indoor positioning.

3.1 System description

The system is managed by an Android application running on a smartphone that computes the location data and merges it with the EEG raw data, acquired by the same dedicated hardware board described in Sec. 2.6.1. The board is composed by a 24-bit ADC, a Cortex-M4 microcontroller and a Bluetooth module for communication with the smartphone. The smartphone obtains the positioning data using IndoorAtlas SDK version 2.2.4, with an accuracy of 1 to 3 m [91]. After the preliminary setup phase, where the cloud builds a map of the magnetic field of the floorplan (fingerprint), device localization is achieved by streaming to the cloud the magnetometer values.

3.1.1 Android app

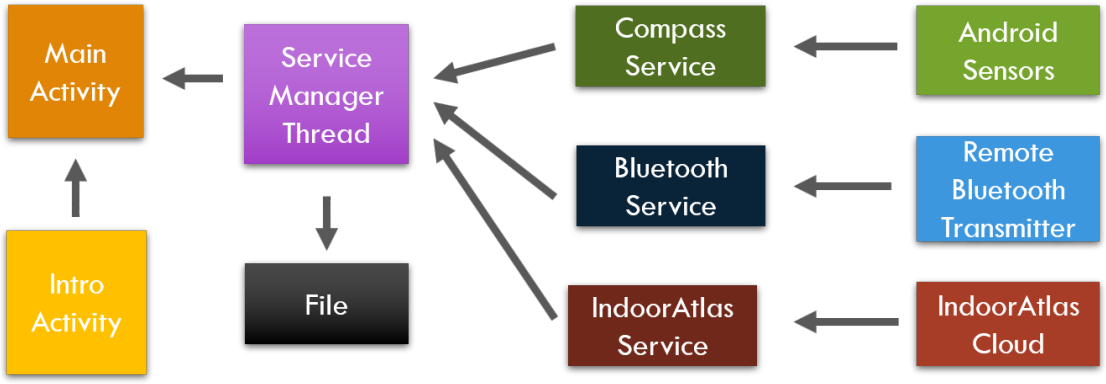

Figure 3.1: Android app architecture

The Android app architecture is depicted in Fig. 3.1. An introductory activity welcomes the user and let him/her choose a paired Bluetooth device, then the main activity starts and immediately spawns the ServiceManager thread. The ServiceManager in turn

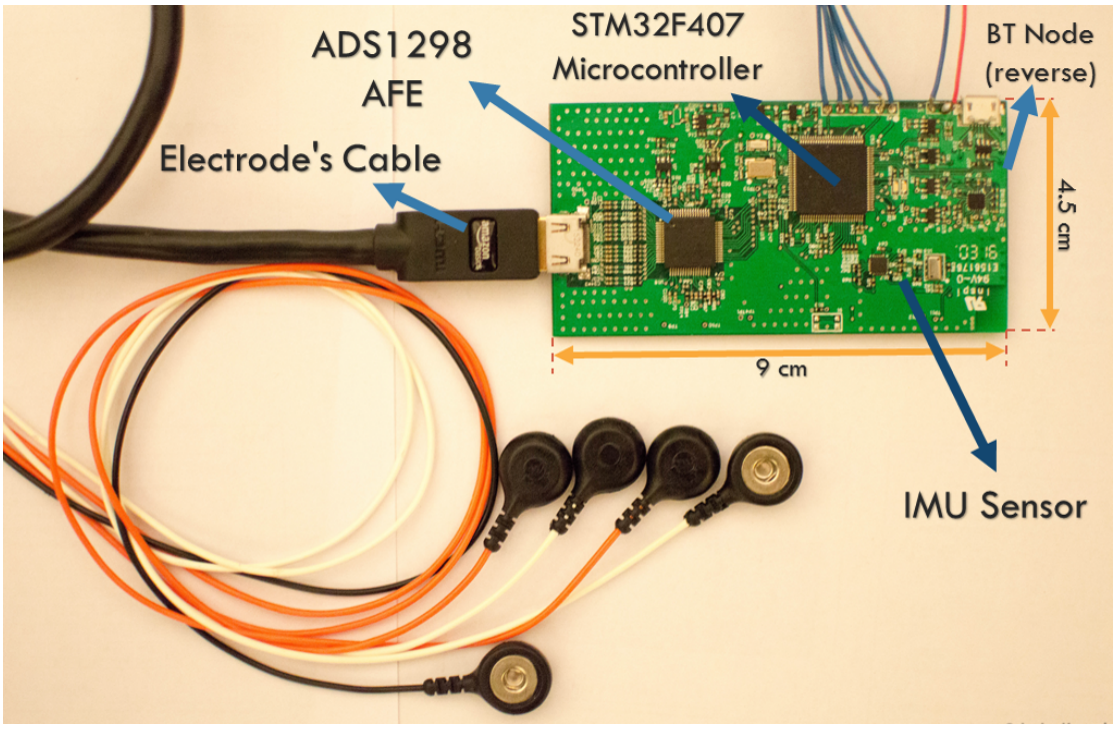

Figure 3.2: EEG acquisition board

generates three services, each one in charge of collecting a part of the dataset: the Bluetooth Service is designed to connect with the paired Bluetooth device and receive EEG data packets of 11 bytes at 500 Hz; the Compass Service is designed to compute orientation through smartphone magnetometer and accelerometer; the IndoorAtlas Service is designed to receive the device position data from the IndoorAtlas cloud. Since all services must be active during the whole application execution, each service spawns a dedicated thread for its long-running task, in order not to burden the ServiceManager with high frequency callbacks. Each dedicated thread stores the received data in an internal thread-safe buffer, together with a timestamp. The ServiceManager periodically accesses the three buffers and retrieves data in the current time window using the timestamp information. Then, the ServiceManager performs synchronization of the data received from the three service sources and attaches, for each Bluetooth data entry, the respective device position and orientation. Such merged and synchronized data is then stored locally in a file for further offline processing.

3.1.2 EEG acquisition system

The EEG signals are acquired with the system implementation presented in Fig. 3.2 [92] [93]. The EEG signals are sampled using the 8-channel Texas Instrument ADS1298 low power analog-to-digital converter, designed for the acquisition of biopotentials (ExG). Each channel has a resolution of 24 bits with a power consumption of 0.75

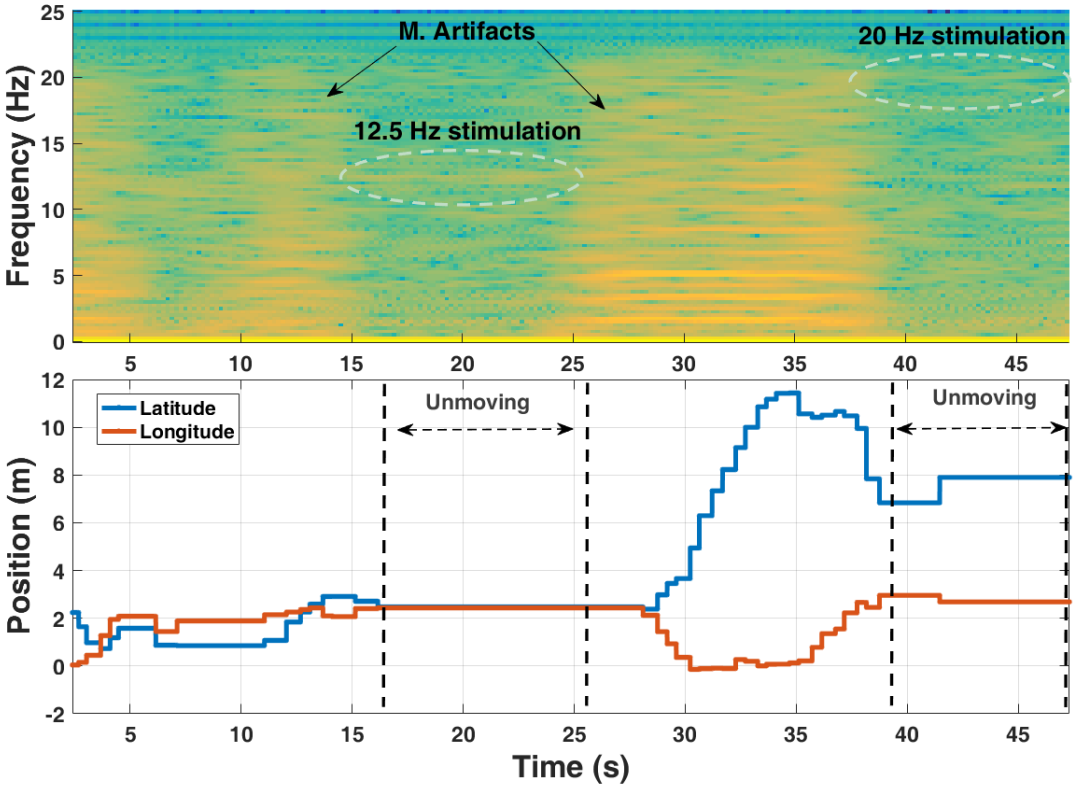

Figure 3.3: Spectrogram of the EEG data and positions

mW. The sampling rate ranges from 250 Hz to 32 kHz. The current system uses only three channels at 500 Hz, located at Oz, Pz and P4, according to the 10-20 reference system [94], with a common reference to A1 (left earlobe) and GND connected to Fz. Circular gel-based electrodes with a surface contact of 2 cm^2 are used to transfer the signals from the skin to the ADC. All the sampled data is then transmitted to a microcontroller via SPI. The STMicroelectronics STM32F407 microcontroller purveys the required computational power. It is based on an ARM Cortex-M4 core running at 168 MHz, with floating point unit, 192 kB of SRAM and 1 MB of non volatile Flash memory. Finally, the raw data is transmitted to the Android application using the Bluegiga WT12 Bluetooth Class 2 Module.

These components populate a 9 × 4.5 cm 6-layer Printed Circuit Board (PCB) as shown in Fig. 3.2. The board's power supply is managed by a dedicated integrated circuit with an internal switching voltage regulator and Low-dropout (LDO) regulators.

3.1.3 Signal processing

The recorded data is analyzed using initially a time-frequency domain transformation. The spectrogram of the signal is computed to visualize the position/frequency relation over time. For this, the EEG data is down-sampled to 100 Hz. Fig. 3.3 is

obtained using the spectrogram function (Matlab) with window size of 100 samples and 50% overlap. It is plotted in relation to the cartesian coordinates in m from a corner of the corridor. The points where the position remains unchanged reveal the moments where the subject is receiving the visual stimulation (10 seconds approximately). Since the quality of the spectrogram is not sufficient to correctly quantify the VEPs, the sections containing the visual stimulation are extracted for a thorough analysis. Given the time-locked nature of the stimuli, signal averaging (on a given time window) is used to increase the signal-to-noise ratio of the segment. Subsequently, the window is analyzed using the Frequency Tagging Analysis (FTA) by average of the frequency components of small chunks of the original signal.

3.1.4 Challenges

Table 3.1: Comparison between different electrode placement

Conf	SNR (SSVEP)	PLI[1]	BA[2]	MA[2]
A	3.14	3.26	9.29	129.25
B	4.65	2.24	39.03	130.29
C	4.10	2.80	8.70	115.21

[1]Measured in Vrms

The major challenge regarding the Android application is data synchronization between services. In fact, there is no practical way to determine via software the arrival time of a Bluetooth packet with ms precision. The Bluetooth unit of the smartphone stores locally the received packets and delivers them to the Android Bluetooth adapter in batches. The frequency of the batch delivery to the Android Bluetooth adapter depends not only on the remote Bluetooth transmission frequency, but also on the internal implementation of the two units. To overcome this problem, an algorithm is devised to estimate the arrival time of one packet and then the transmission frequency knowledge is exploited to update the timestamp for each following packet.

Regarding the acquisition of the EEG signals, challenges arise because of the different sources of noise. These are normally lessened by carrying out experimentation in carefully controlled environments. Mainly, three sources of interference are present during the recordings. The first corresponds to the movement artifacts (MA), caused by the movement of the electrode and/or the electrical changes due to energy equalization between the subject and the ground. The second, the blink artifacts (BA), normally present in EEG measurements, are generated by the movement of the eyes. The third corresponds to the 50 Hz power line interference (PLI). While recording on real-life scenarios, the location of the electrodes plays an important role in reducing the effects of the mentioned artifacts, but simultaneously, it can also affect the amplitude of the

studied signal. Since SSVEP are mostly present at the right side of the occipital lobe [95]. The use of three electrodes on this region balances complexity and the likelihood of capturing the signal.

The reduction of artifacts is finally achieved after selecting a proper electrode placement. Empirical experimentation was performed to quantify the PLI, BA and MA interference in three different configurations. These are: GND and all reference electrodes connected to A1 (A), GND at Fz and all references at connected to the Fp1 (B) and GND at Fz and all references connected to A1 (C). Table 3.1 shows the results of the experimentation, demonstrating that C rejects successfully more noise than the other configurations, notwithstanding that it does not have the best SNR.

3.2 Experiments and results

3.2.1 Experimental setup

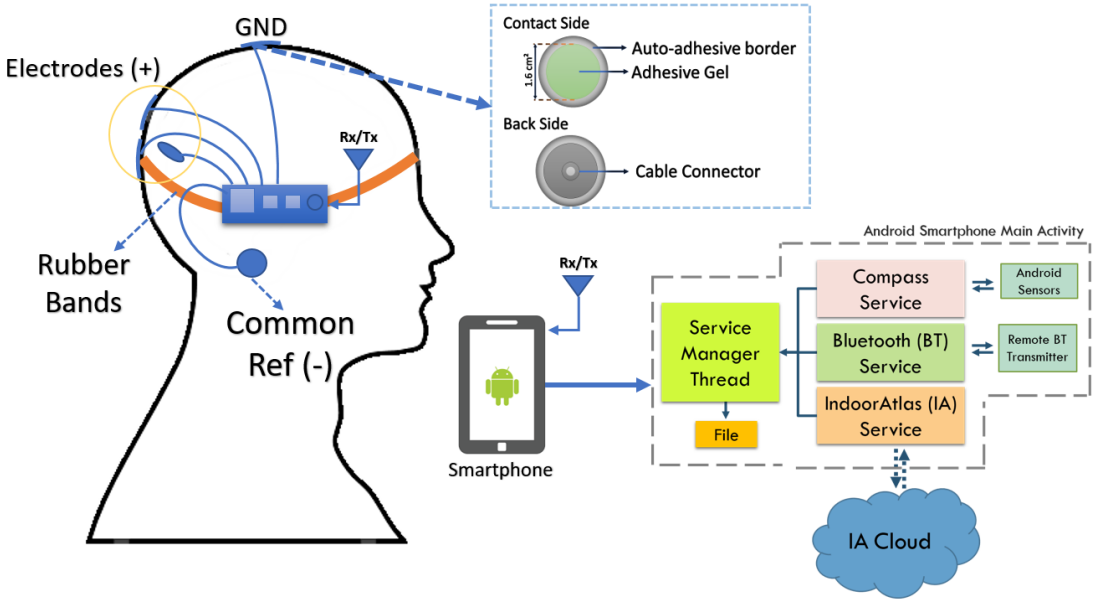

Figure 3.4: Overview of the full wearable system composed by the BCI board and electrodes placed on the head, and the Android hand held device.

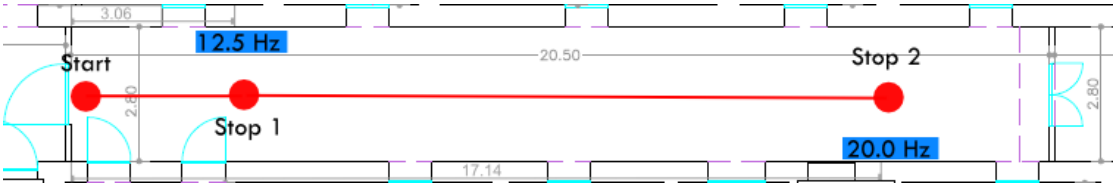

Figure 3.5: Predefined path and stimuli location

The system described in Sec. 3.1 is tested on one healthy subject with no previous history of neural diseases. The board is placed on the subject's head, as shown in Fig.

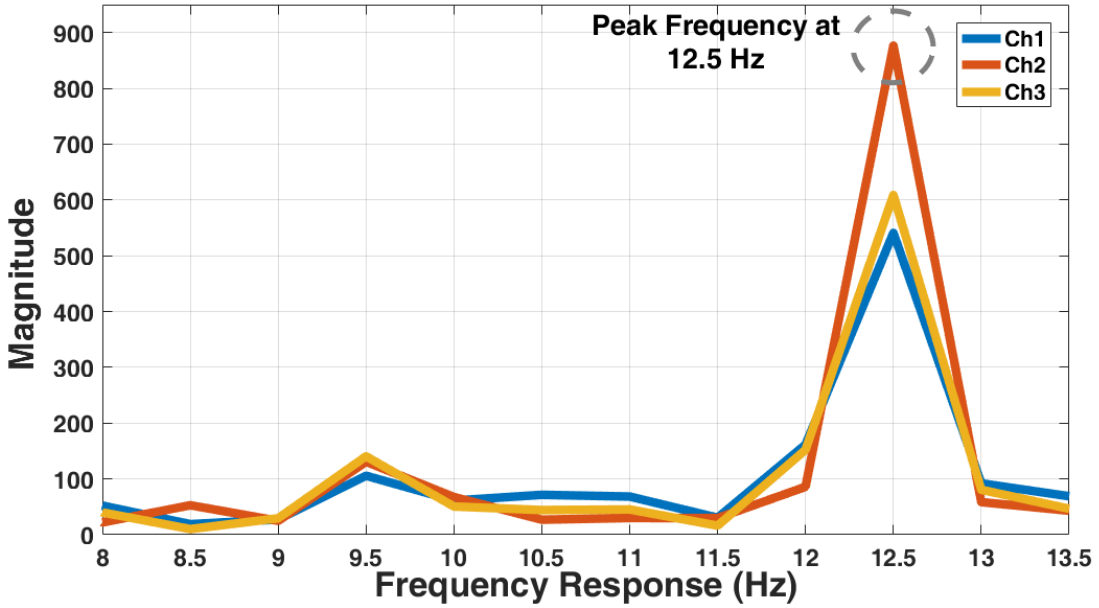

Figure 3.6: Frequency Response for SSVEP at 12.5Hz.

3.4. The electrodes are located at Oz, Pz and P4, following the 10-20 reference system, while the reference electrode was placed at Fz.

The subject was asked to follow the predefined path as indicated in Fig. 3.5. The visual stimulation is presented along the walking path by two identical Full High-Definition (HD) screens (15", 1920x1080px) with a refresh rate greater than 60 FPS. The distance between the screen and the user during the stimulation is about 1 meter. The visual stimulation is generated using a checkerboard (10x10 square elements) covering 35% of the screen over a grey background. In this experiment, the first stimulus on the path is at 12.5 Hz, wile the second is at 20 Hz.

The subject explores the walking path from the starting point. Once the first screen is reached, the subject observes the screen with the corresponding visual stimulation to generate the SSVEP. Subsequently, the user moves to the next screen for the last stimuli observation. The subject's position and EEG data is recorded using the implementation presented in Sec. 3.1.2 and 3.1.3 for posterior offline analysis.

3.2.2 Experimental results

The resulting raw data is processed following the methodology presented in Sec. 3.1.3. The two plots presented in Fig. 3.6 and Fig. 3.7 reveal the capability of the system to detect the generated stimuli. It is worth noticing also that the channel carrying the strongest frequency response is not always the same, specially for different frequencies, which justifies the employment of multiple electrodes.

As an another study case using the proposed platform, the focus was set on the

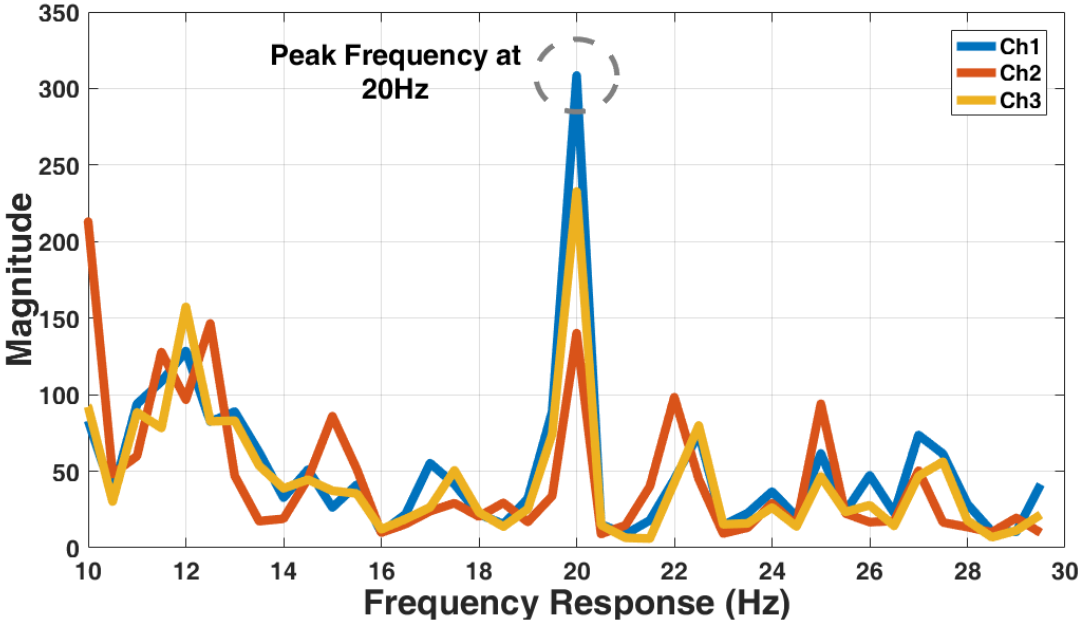

Figure 3.7: Frequency Response for SSVEP at 20Hz.

Table 3.2: Relation between the subject speed and the frequency of the movement artifacts. The growing trend suggests a correlation between the two measures.

Velocity(Km/h)	CF1[2]	CF2	CF3
3.02	1.4	2.8	4.3
3.4	1.5	3.1	4.7
4.35	1.6	3.5	5
5.1	1.9	3.6	5.1

[2]Central Frequency (CFx) measured in Hz

correlation between the moving artifacts and the displacement of the subject. Fig. 3.3 shows the frequency components of the artifacts featuring three spectral lines components with a bandwidth of 1 Hz and a separation of 1.5 Hz approx. Table 3.2 shows the results of experimentation with different increasing walking speeds, where is worth notice that these lines have the tendency to move towards higher frequencies. This characterization may be useful to develop a method to determine the speed of the user or to reduce the effects of these artifacts. This may be covered in a future research.

In summary, the current results show that the Evoked Potentials can be successfully extracted using the proposed system even in a mobile, wearable setup (as opposed to the usual stationary conditions used in EEG experiments). This encourage the belief that the current platform will enable us to seek for more complex brain responses in a future research. Also, correlations between indoor position and motion were characterized, which can be used to extract extra information from the signal or to increase the SNR, demonstrating significant opportunity for sensor fusion exploiting real-time

location and EEG tracking. Moreover, the system can be applied for studying the environmental context such as the visibility of the stimuli, the presence of other persons obstructing the stimuli, or the interest of one person to stare at a particular portion of the wall, with possible applications in exposition contexts like stores or museums. It is worth mentioning that all the data-set generated so far and in future experimentations will be publicly available, enabling other researchers to study the brain activity in relation with position. Another important contribution of this work is that all the data is collected in real scenarios. This will challenge the current methods but will empower the development of new algorithms to mitigate the effects of undesired signals present in the environment.

Chapter 4

AR-based BCI

Despite BCIs moving towards being embedded in wearable devices, visual stimuli are still mostly presented on large LCD monitors, limiting their application to fixed locations of the environment. By combining BCIs with AR tools such as smart glasses, microprojectors or head-mounted displays (HMD), the system flexibility can be dramatically increased. As an example, visual stimuli can be triggered adaptively according to the user's position or action. So, if the user approaches a specific object, a BCI starts to interact with that object through the HMD.

An example of the integration of a P300 based BCI system used to enable HMI is reported in [96], where an EEG acquisition system is coupled with an AR system to enable the control of a smart home. The system is tested on three subjects for tasks of domotic control (i.e. TV channel switching, opening and closing doors.). The subjects were firstly trained in numbers and characters spelling based on their P300 response. The final needed time for recognition task is typically around 30s with accuracy ranging from 83 to 100%. This system reaches high accuracy but it is intended for users with severe disabilities, based on a full coverage EEG cap and not suitable for a wearable consumer application.

The work of [97] presents a wearable interface that combines an eye-tracker with a BCI trigger to detect the response to visual stimulation using a binary classifier. Basically, the eye-tracker detects where the user is looking, and enables the SSVEP stimuli mapped on the intended object, enabling the user to choose how to interact with the object. The system is based on a modified version of the Emotiv NeuroHeadset, using wet saline electrodes which acquire the EEG signal at 128 Hz. Samples are sent wirelessly to an Odroid board, powered by a high-end processor (i.e. Samsung Exynos4412 Prime chip operating with 1.7 GHz ARM Cortex-A9 Quad Cores). The average classification accuracy is 73.5% while the time needed to perform a recognition task is higher than 4 seconds.

Another solution, presented in [98], relies on a simpler approach, since it uses a QR code recognition to enable the interaction with the selected object and a commercial smart glasses system [99] to present the SSVEP stimuli. The embedded camera of the eyeglasses executes a QR-code recognition when the user is looking in the direction of the intended object, and enable the SSVEP stimulation accordingly. The EEG data are acquired with an Emotiv EEG neuroheadset, and processed by a bench top host PC. This system was tested on 7 subjects reaching an average accuracy of 85.7% with a recognition latency that ranges from 3 to 6 seconds. The aforementioned solutions are inspiring attempts to enable a natural, hand and voice free control strategy, but they are based on bulky setups, where the EEG interface requires skin preparation and the digital computing platforms are power-hungry and cumbersome, hence not suitable to be integrated into an unobtrusive wearable form factor.

This chapter shows how to enhance the embedded wearable BCI discussed in Chapter 2 by connecting the device with commercial smart glasses (Moverio BT-200 [99]), which provides the visual stimuli exploiting AR techniques. This solution allows for a fully-wearable self-contained plug-and-play BCI with a wide range of possible applications in industrial and smart-home scenarios. The enhanced system is tested on five subjects, reaching an average accuracy of 80% with a recognition latency of 3 seconds, suitable for a fast and reliable BCI.

4.1 Smart glasses

The HMD used for AR stimuli presentation is the EPSON Moverio BT-200, a commercial smart glasses running Android 4.0.4 on a dual-core ARM Cortex A9. The device allows for WiFi and Bluetooth connectivity. The display is a TFT active matrix with LCD size of 0.42 inches, 16:9 aspect ratio and 60 Hz refresh rate. The viewer, a binocular see-through that renders a screen of 80 inch virtual size at a virtual distance of 5 m, makes Moverio BT-200 particularly suitable for 3D AR applications. The processor and battery are enclosed in a handheld trackpad for standard interaction. The see-through display of Moverio BT-200 is a particularly desirable feature, since it allows the user to interact directly with the real world when virtual augmentation is not necessary, and let the user see both real world and information overlay whenever augmentation is needed.

4.2 AR for stimuli presentation

Using the integrated camera and Vuforia SDK for digital eyewear [100], a BCI App is developed that detects whenever the user is staring at tags, which can be freely applied

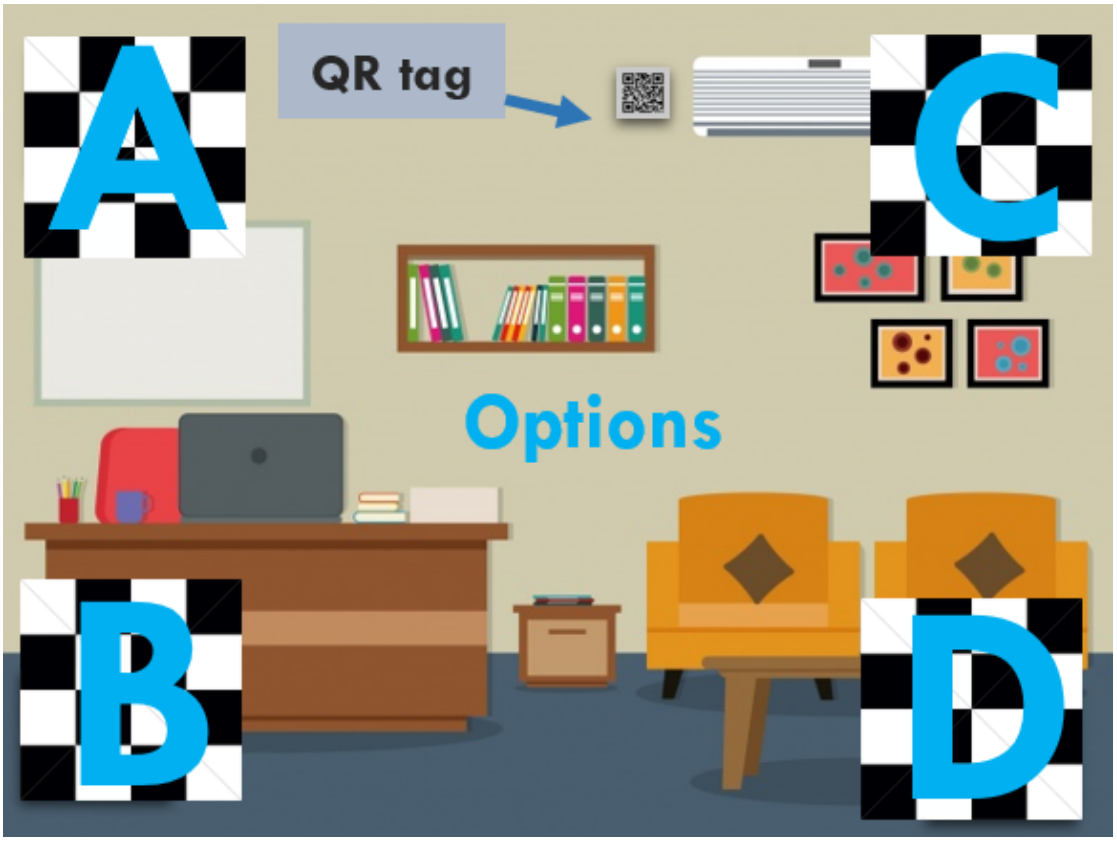

Figure 4.1: Example of the application usage from the user's perspective.

to objects in the environment, and informs the BCI wearable node that the user wants to interact with a certain object. Different tags can trigger different numbers of stimuli but, remarkably, different tags can trigger stimuli using the same set of frequencies, overcoming the bottleneck problem of pushing as many target frequencies as possible in a small bandwidth between 5 Hz and 10 Hz, where the SSVEP response is maximized. Each stimulus consists of a PNG image representing an 8 x 8 black and white square checkerboard, with a gray diagonal cross to guide user's gaze. The frequency of the stimulus is rendered by modulating the image opacity from 0 to 1 with a sine waveform. The app can dynamically arrange up to six different checkerboards at the same time, however in this work the focus is on a four checkerboard setup. Each checkerboard is controlled by its own ValueAnimator object, initialized for linearly animating float values from 0 to 2, representing the coefficient of π in the sine wave equation. The duration of the animation reflects the stimulus frequency, and it is computed from the frequency attribute, which can be set directly in the XML layout file. An AnimatorUpdateListener object is used to intercept the updates of the ValueAnimator animation, and set the opacity of the image accordingly. The animation is then repeated for a number of times calculated on the predefined stimulation length, and then the checkerboard disappears. Fig 4.1 shows an example of the application usage from the user's perspective: when the user looks at a tag, four flickering checkerboards appear on the HMD, representing

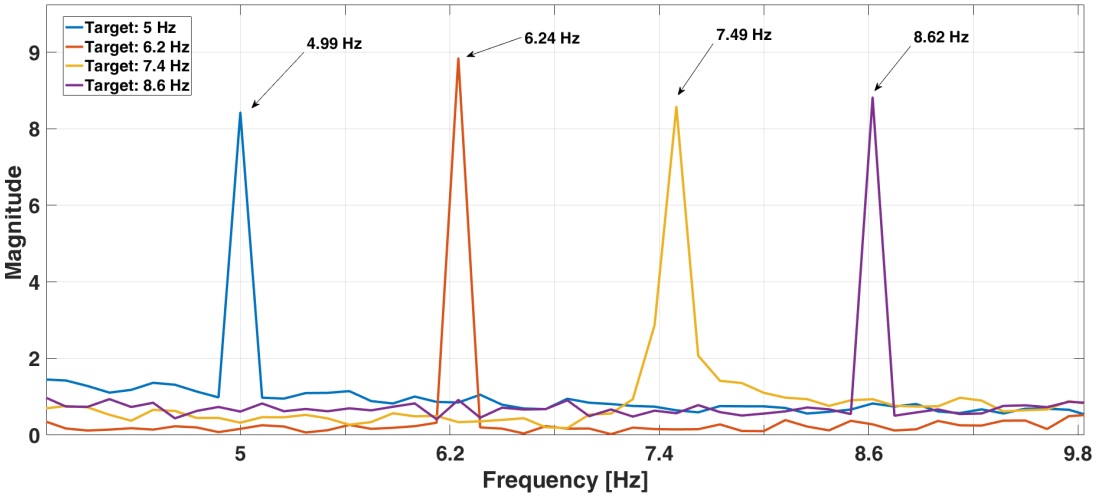

Figure 4.2: Frequency response of stimuli generated on the AR glasses and captured by a photo-resistor. The deviation from the target frequency is < 0.1 Hz.

four possible actuations on the corresponding item. The app notifies via Bluetooth the BCI wearable node when stimulation begins and ends, allowing the MCU to execute the classification algorithm only when SSVEP can be detected, significantly reducing power consumption.

4.3 AR-based stimuli validation

The BCI system has been validated on five healthy subjects (aged 25-43), with normal or corrected-to-normal vision. All participants reported no history of neurological or psychiatric disorders and provided written consent to participate in the experiments. The tests have been carried out in an lab environment, which is particularly harsh in terms of electrical and electromagnetic noise.

The first test is intended to validate the stimulus presentation described in 4.2. To this end, a photo-resistor is connected to one input of the system, to capture light variations generated by the projection of the flickering checkerboards on the glasses. Fig 4.2 shows the Power Spectral Density (PSD) of the resulting signal, indicating that the maximum deviation from the original target frequency is confined below 0.1 Hz. Such variations do not affect the final accuracy of the system for time windows up to a few seconds. It is possible to note that the peak corresponding to 7.4 Hz is not as sharp as the others. This may be due to noise or movement artifacts of the light sensor during the presentation of the 7.4 Hz stimulus, since it is hand held near one of the smart glasses lenses.

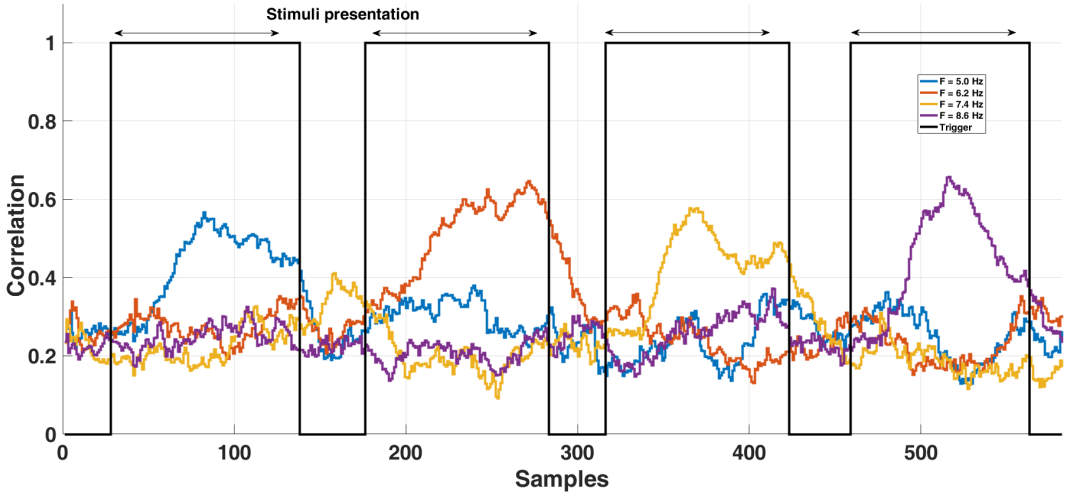

Figure 4.3: CCA correlation

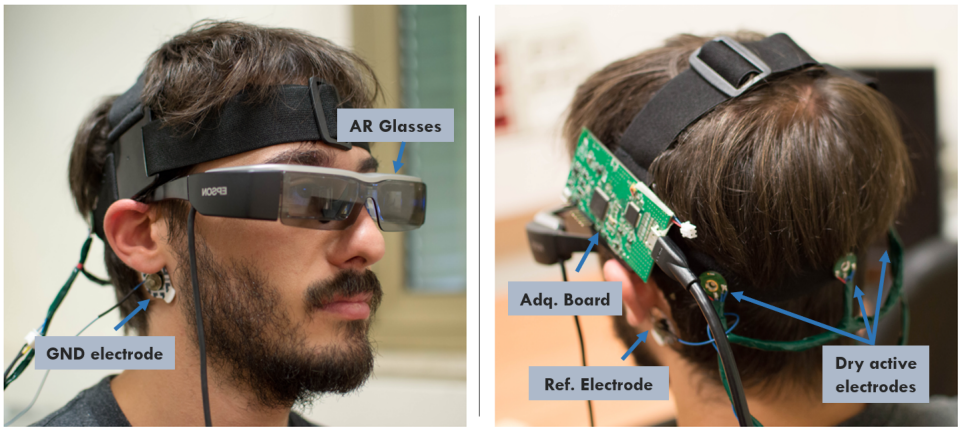

Figure 4.4: Front and back view of the complete setup during a test.The HDMI cable attached to the board is used only for testing purpose, and it is not required during normal operation of the system. Similarly, the current size and weight of the PCB allow an easy debugging. Nevertheless, the entire hardware dimensions can be reduced to a half.

4.4 Experiments and results

4.4.1 Experimental setup

SSVEP signals are elicited employing four black and white checkerboards as described in Sec. 4.2, arranged in a 2 x 2 pattern, located at the corners of the visual field of the smart glasses display. Four equally spaced frequency-coded stimuli (5.0 Hz, 6.2 Hz, 7.4 Hz and 8.6 Hz) are used as targets. During the tests, the subjects will fix the eyesight at a target indicated with a red cue before the onset of the stimulation. Later, all the stimuli will remain active for ten seconds, followed by 5 seconds of pause

to reduce visual fatigue. This process is repeated four times to cover all checkerboards, and the trial is repeated three times for each subject.

Concurrently, EEG data is acquired using the hardware presented in Sec. 2.2.2 and 2.6.1 from three electrodes placed at the occipital lobe (P5, POZ, and P6), with reference and ground located at A1 and A2 respectively. An example of the complete setup is presented at Fig. 4.4.

Before each test with the smart glasses, a control test is performed using a regular 24-inch LED (60fps) display. The results obtained are later used to evaluate the performance of the AR projections with respect to the classical technique for SSVEP stimulation [101].

4.4.2 Experimental results

Subject	Latency (s)	Accuracy	ITR (b/s)
S1	2.57	1.00	0.78
	4.50	1.00	0.44
	3.08	1.00	0.65
S2	2.95	0.67	0.19
	3.85	0.91	0.37
	2.25	1.00	0.89
S3	3.03	0.63	0.15
	3.78	0.68	0.16
	2.00	0.87	0.62
S4	1.70	0.91	0.83
	3.13	0.85	0.37
	1.58	0.82	0.65
S5	5.63	0.69	0.11
	3.00	0.50	0.07
	2.50	0.50	0.08
Average	**3.04**	**0.80**	**0.42**

Table 4.1: Experimental results. For each subject results of three trials are reported.

Table 4.1 reports detailed results for all subjects. To account for some occasional variabilities regarding the acquisition setup each subject has repeated the test three times. Of the five subjects, only S5 has performed poorly, possibly due to a certain degree of intolerance to bearing the eyeglass frames. Nevertheless, the average results show that the system is reliable (average accuracy 80%) and responsive (average latency of about 3 s), with an average ITR with four targets of 0.42 b/s.

The results demonstrate that the presented embedded implementation outperforms systems based on AR eyeglasses while being also aligned with the SoA traditional SSVEP systems. Moreover, this work shows that online and real-time processing is achievable

through a low-intrusivity setup, which is a significant step forward with respect to the current offline and bulky systems.

Chapter 5

Conclusions

This dissertation presents a novel SSVEP embedded BCI system based on a custom hardware platform for medical IoT and a minimally intrusive setup with 3 zero-preparation EEG dry electrodes. Leveraging a multimodal approach, which ranges from EEG acquisition to embedded optimization, this work aims at widening the usage of BCI systems among able-bodied people, by designing a fully wearable and easy-to-use system for brain-machine communication with up to eight stimuli. The work goes a step further combining a deeply embedded platform with dry electrodes, which highlights the contribution of this work with regards of current system based on cumbersome processing platforms and wet electrodes. The whole processing chain, from raw EEG signal acquisition to frequency identification via CCA algorithm, is executed in real-time on an embedded cost-effective microcontroller. The code optimization, tailored for the CORTEX M4 Instruction Set Architecture allows to calculate up to 10 EEG feature classifications per second, keeping power consumption as low as 27.5 mW. The system has been fully designed, tested and validated on five subjects, achieving an average ITR of 1.06 b/s with the dry electrodes interface and 1.28 b/s with the wet electrodes interface. The proposed solution does not require subject dependent training and synchronization mechanisms for the stimuli presentation, hence it is suitable for the deployment in non-prepared environment.

In the third chapter, the same hardware is used in a study for combining EEG signals with subject position data retrieved with a smartphone via indoor positioning system. Differently form the setup in the second chapter, this time the system features only wet electrodes and the results are analyzed offline. The system is tested in a real environment and experimental results show that it is possible to extract Evoked Potentials from the EEG signal and therefore locate the subject.

In the fourth chapter is presented the enhancement of the BCI system described in the second chapter, resulting in a fully-wearable BCI composed of a low-power EEG

acquisition system for SSVEP detection connected to a pair of commercial smart glasses for stimuli presentation. The use of AR environment delivers a realistic BCI, promising a more intuitive way of brain communication. The wearable BCI offers the performance of the current SoA systems while also providing a real-time EEG signal classification through a non-intrusive, embedded processing platform. The system has been validated on five subjects, achieving an average ITR of 0.42 b/s and an average output latency of 3.0 seconds. This performance substantially improves those of SoA wearable systems employing AR and smart glasses in terms of both accuracy and delay [97, 98]. Firmware optimization of the algorithm has been shown helpful in keeping power consumption as low as 32.12 mW, essential for providing extended hours of operation. The usage bottleneck of the system is therefore constituted by the battery duration of the commercial HMD device.

This work aims at spreading the usage of BCI systems by devising a wearable easy-to-use online system ready to be deployed in fields where reliability constraints are stronger, such as smart environments like industry 4.0. The ability of the proposed system to provide a real-time user experience highlights the contribution of this work towards a more realistic and useful BCI. It is already possible to envision some future enhancements to the current system, under hardware and software point of view. As a first remark, the commercial smart glasses used for stimuli augmentation represent a bottleneck for power consumption, hindering the long term usage capability of the BCI. To overcome this problem, future work can follow two possible scenarios: acting on the smart glasses device hardware, or acting on the BCI configuration. In former case, a careful hardware design for a custom low power smart glasses device is required. In latter case, another BCI based on mu or beta rhythm, or EOG, can be used to control stimuli activation. Unlike the current system, where the smart glasses camera is active all the time and the device is performing continuous pattern recognition, in this scenario the stimuli presentation is triggered by the low power BCI, and the power hungry smart glasses can be kept idle for the remaining time. The BCI in this configuration must implement two behavioural states: regular SSVEP-based classification during stimuli presentation and "start stimuli command" detection the rest of time. The command can be encoded into a double eyeblink and decoded using EOG, or with a brain rhythm pattern like mu, beta or alpha waves. In case of EOG encoding, at least one more electrode is needed near the forehead to capture the eye blinking, whereas in case of alpha, beta and mu waves the user might need training to learn how to produce the required pattern.

Hardware upgrade can be done also for the BCI device, by porting the firmware on a Parallel Ultra Low Power (PULP) architecture [102]. Switching to such architecture would bring an advantage in the power consumption over performance trade-off of the system, making room for a better suited and more performing classifiers than simple

threshold. In particular, Convolutional Neural Networks have been proven to be good classifiers for SSVEP-based dry electrodes BCI [103], and it would be interesting to test their performance on a minimal invasive and wearable setup like the one discussed in this thesis. As a further investigation, it would be interesting to assess the value of ITR on varying number of stimuli and number and position of channels. Such characterization could clarify the trade-offs between performance, electrodes, and stimuli, helping BCI designers to choose the most suitable configuration for their target application.

Bibliography

[1] Angela T Chan, Juan C Quiroz, Sergiu Dascalu, and FC Harris. An overview of brain computer interfaces. In *Proc. 30th Int. Conf. on Computers and Their Applications*, 2015.

[2] Thalmic Labs. Thalmic's MYO Armband. URL `https://www.myo.com/`.

[3] Gernot R Muller-Putz and Gert Pfurtscheller. Control of an electrical prosthesis with an SSVEP-based BCI. *IEEE Transactions on Biomedical Engineering*, 55(1): 361–364, 2008.

[4] Kai Keng Ang et al. Brain-computer interface-based robotic end effector system for wrist and hand rehabilitation: results of a three-armed randomized controlled trial for chronic stroke. *Frontiers in neuroengineering*, 7:30, 2014.

[5] Phoebe Weston. Battle for control of your brain: Microsoft takes on Facebook with plans for a mind-reading HEADBAND that will let you use devices with the power of thought. *Mail Online*, 2018. URL `http://www.dailymail.co.uk/sciencetech/article-5274823/Microsoft-takes-Facebook-mind-reading-technology.html`.

[6] Sarah Marsh. Neurotechnology, Elon Musk and the goal of human enhancement. *The Guardian*, 2018. URL `https://www.theguardian.com/technology/2018/jan/01/elon-musk-neurotechnology-human-enhancement-brain-computer-interfaces`.

[7] Kristen V. Brown. Here Are the First Hints of How Facebook Plans to Read Your Thoughts. *Wired*, 2018. URL `https://gizmodo.com/here-are-the-first-hints-of-how-facebook-plans-to-read-1818624773`.

[8] VeeaR, Global Industry Analysts, Inc. (GIA), 2018. URL `http://www.veear.eu/`.

[9] Google Inc. Google glass. URL `https://x.company/glass/`.

[10] Mindmaze. Mindmaze Mask, 2018. URL `https://www.mindmaze.com/mask/`.

[11] Neurosky. Neurosky MindWave, 2018. URL `http://neurosky.com/biosensors/eeg-sensor/biosensors/`.

[12] Emotiv, 2018. URL `https://www.emotiv.com/`.

[13] OpenBCI, 2018. URL `http://openbci.com/`.

[14] g.tec GmbH. g.tec Intendix, 2018. URL `http://www.gtec.at/Products/Complete-Solutions/intendiX-Specs-Features`.

[15] Donghee Son et al. Multifunctional wearable devices for diagnosis and therapy of movement disorders. *Nature nanotechnology*, 9(5):397, 2014.

[16] Gert Pfurtscheller et al. The hybrid BCI. *Frontiers in neuroscience*, 4:3, 2010.

[17] T Klingeberg and Marcel Schilling. Mobile wearable device for long term monitoring of vital signs. *Computer methods and programs in biomedicine*, 106(2):89–96, 2012.

[18] M. Hooshmand et al. Boosting the battery life of wearables for health monitoring through the compression of biosignals. *IEEE Internet of Things Journal*, 2017.

[19] A. A. Abdellatif et al. EEG-based Transceiver Design with Data Decomposition for Healthcare IoT Applications. *IEEE Internet of Things Journal*, pages 1–1, 2018. doi: 10.1109/JIOT.2018.2832463.

[20] Luis Fernando Nicolas-Alonso and Jaime Gomez-Gil. Brain computer interfaces, a review. *Sensors*, 12(2):1211–1279, 2012.

[21] Muhammad Bilal Khalid, Naveed Iqbal Rao, Intisar Rizwan-i Haque, Sarmad Munir, and Farhan Tahir. Towards a brain computer interface using wavelet transform with averaged and time segmented adapted wavelets. In *Computer, control and communication, 2009. ic4 2009. 2nd international conference on*, pages 1–4. IEEE, 2009.

[22] Jonathan R Wolpaw, Niels Birbaumer, Dennis J McFarland, Gert Pfurtscheller, and Theresa M Vaughan. Brain–computer interfaces for communication and control. *Clinical neurophysiology*, 113(6):767–791, 2002.

[23] Thomas Elbert, Brigitte Rockstroh, Werner Lutzenberger, and Niels Birbaumer. Biofeedback of slow cortical potentials. i. *Electroencephalography and clinical neurophysiology*, 48(3):293–301, 1980.

[24] Niels Birbaumer, Nimr Ghanayim, Thilo Hinterberger, Iver Iversen, Boris Kotchoubey, Andrea Kübler, Juri Perelmouter, Edward Taub, and Herta Flor. A spelling device for the paralysed. *Nature*, 398(6725):297, 1999.

[25] Niels Birbaumer, Andrea Kubler, Nimr Ghanayim, Thilo Hinterberger, Jouri Perelmouter, Jochen Kaiser, Iver Iversen, Boris Kotchoubey, Nicola Neumann, and Herta Flor. The thought translation device (ttd) for completely paralyzed patients. *IEEE Transactions on rehabilitation Engineering*, 8(2):190–193, 2000.

[26] Gert Pfurtscheller, Ch Neuper, Doris Flotzinger, and Martin Pregenzer. Eeg-based discrimination between imagination of right and left hand movement. *Electroencephalography and clinical Neurophysiology*, 103(6):642–651, 1997.

[27] Hui Shen, Li Zhao, Yan Bian, and Longteng Xiao. Research on ssvep-based controlling system of multi-dof manipulator. In *International Symposium on Neural Networks*, pages 171–177. Springer, 2009.

[28] Xiaorong Gao, Dingfeng Xu, Ming Cheng, and Shangkai Gao. A bci-based environmental controller for the motion-disabled. *IEEE Transactions on neural systems and rehabilitation engineering*, 11(2):137–140, 2003.

[29] William M Perlstein et al. Steady-state visual evoked potentials reveal frontally-mediated working memory activity in humans. *Neuroscience letters*, 342(3):191–195, 2003.

[30] David E Thompson, Stefanie Blain-Moraes, and Jane E Huggins. Performance assessment in brain-computer interface-based augmentative and alternative communication. *Biomedical engineering online*, 12(1):43, 2013.

[31] Sylvain Baillet, John C Mosher, and Richard M Leahy. Electromagnetic brain mapping. *IEEE Signal processing magazine*, 18(6):14–30, 2001.

[32] Saeid Sanei and Jonathon A Chambers. Eeg signal processing. 2007.

[33] COVIDIEN. Covidien Kendall, 2015. URL `https://bio-medical.com/covidien-kendall-disposable-surface-emg-ecg-ekg-electrodes-1-3-8-35mm-50pkg.html`.

[34] g.tec GmbH. g.SAHARA. URL `http://www.gtec.at/Products/Electrodes-and-Sensors/g.SAHARA-Specs-Features`.

[35] Masaki Nakanishi et al. Enhancing Detection of SSVEPs for a high-speed brain speller using task-related component analysis. *IEEE Transactions on Biomedical Engineering*, 65(1), 2018.

[36] Xiaogang Chen et al. High-speed spelling with a noninvasive brain–computer interface. *Proceedings of the national academy of sciences*, 112(44):E6058–E6067, 2015.

[37] Xiaogang Chen, Zhikai Chen, Shangkai Gao, and Xiaorong Gao. A high-ITR SSVEP-based BCI speller. *Brain-Computer Interfaces*, 1(3-4):181–191, 2014.

[38] Hsiang-Chih Chang et al. Real-time control of an SSVEP-actuated remote-controlled car. In *SICE Annual Conference 2010, Proceedings of*, pages 1884–1887. IEEE, 2010.

[39] Martin Spüler. A high-speed brain-computer interface (BCI) using dry EEG electrodes. *PloS one*, 12(2), 2017.

[40] Niccolò Mora et al. Plug&play brain–computer interfaces for effective active and assisted living control. *Medical & biological engineering & computing*, 55(8):1339–1352, 2017.

[41] Hubert Cecotti. A self-paced and calibration-less SSVEP-based brain–computer interface speller. *IEEE Transactions on Neural Systems and Rehabilitation Engineering*, 18(2):127–133, 2010.

[42] Jzau-Sheng Lin and Cheng-Hung Hsieh. A wireless BCI-controlled integration system in smart living space for patients. *Wireless Personal Communications*, 88 (2):395–412, 2016.

[43] PA García et al. An Embedded Hybrid BCI Speller. In *VII Latin American Congress on Biomedical Engineering CLAIB 2016, Bucaramanga, Santander, Colombia, October 26th-28th, 2016*, pages 26–29. Springer, 2017.

[44] Xuhong Guo et al. Developing a one-channel BCI system using a dry claw-like electrode. In *Engineering in Medicine and Biology Society (EMBC), 2016 IEEE 38th Annual International Conference of the*, pages 5693–5696. IEEE, 2016.

[45] Yu Mike Chi et al. Dry and noncontact EEG sensors for mobile brain–computer interfaces. *IEEE Transactions on Neural Systems and Rehabilitation Engineering*, 20(2):228–235, 2012.

[46] M. Salvaro and S. Benatti and V. Kartsch and M. Guermandi and L. Benini. A Minimally Invasive Low-Power Platform for Real-Time Brain Computer Interaction based on Canonical Correlation Analysis. *IEEE Internet of Things Journal*, pages 1–1, 2018. ISSN 2327-4662. doi: 10.1109/JIOT.2018.2866341.

[47] Shravani Sur and VK Sinha. Event-related potential: An overview. *Industrial psychiatry journal*, 18(1):70, 2009.

[48] Lawrence Ashley Farwell and Emanuel Donchin. Talking off the top of your head: toward a mental prosthesis utilizing event-related brain potentials. *Electroencephalography and clinical Neurophysiology*, 70(6):510–523, 1988.

[49] Emanuel Donchin et al. The mental prosthesis: assessing the speed of a P300-based brain-computer interface. *IEEE transactions on rehabilitation engineering*, 8(2):174–179, 2000.

[50] Hilit Serby et al. An improved P300-based brain-computer interface. *IEEE Transactions on neural systems and rehabilitation engineering*, 13(1):89–98, 2005.

[51] Mattia Salvaro, Victor Kartsch, Simone Benatti, Michela Milano, and Luca Benini. Towards a novel hmi paradigm based on mixed eeg and indoor localization platforms. In *CAS (NGCAS), 2017 New Generation of*, pages 217–220. IEEE, 2017.

[52] Alban Duprès et al. SSVEP-based BCIs: study of classifier stability over time and effects of human learning on classification accuracy. *AMSE, Journal of the Association for the Advancement of Modelling and Simulation Techniques in Enterprises (Special edition HANDICAP)*, 2014.

[53] Min Hye Chang et al. Eliciting dual-frequency SSVEP using a hybrid SSVEP-P300 BCI. *Journal of neuroscience methods*, 258:104–113, 2016.

[54] Ming Cheng et al. Design and implementation of a brain-computer interface with high transfer rates. *IEEE transactions on biomedical engineering*, 49(10):1181–1186, 2002.

[55] Robert Prueckl and Christoph Guger. A brain-computer interface based on steady state visual evoked potentials for controlling a robot. In *Bio-Inspired Systems: Computational and Ambient Intelligence*, pages 690–697, Berlin, Heidelberg, 2009. Springer Berlin Heidelberg.

[56] Rajesh Singla and BA Haseena. Comparison of SSVEP signal classification techniques using SVM and ANN models for BCI applications. *International Journal of Information and Electronics Engineering*, 4(1):6, 2014.

[57] Harold Hotelling. Relations between two sets of variates. *Biometrika, JSTOR*, 28 (3/4):321–377, 1936.

[58] Z. Lin et al. Frequency Recognition Based on Canonical Correlation Analysis for SSVEP-Based BCIs. *IEEE Transactions on Biomedical Engineering*, 53(12): 2610–2614, Dec 2006. ISSN 0018-9294. doi: 10.1109/TBME.2006.886577.

[59] Guangyu Bin et al. An online multi-channel SSVEP-based brain–computer interface using a canonical correlation analysis method. *Journal of neural engineering*, 6(4):046002, 2009.

[60] G. Tang et al. Compressed Sensing Off the Grid. *IEEE Transactions on Information Theory*, 59(11):7465–7490, Nov 2013.

[61] J. Ying et al. Hankel matrix nuclear norm regularized tensor completion for n-dimensional exponential signals. *IEEE Transactions on Signal Processing*, 65(14): 3702–3717, July 2017.

[62] Zhonglin Lin et al. Frequency recognition based on canonical correlation analysis for SSVEP-based BCIs. *IEEE transactions on biomedical engineering*, 53(12): 2610–2614, 2006.

[63] Valeria Mondini, Anna Lisa Mangia, Luca Talevi, and Angelo Cappello. Sinc-windowing and multiple correlation coefficients improve ssvep recognition based on canonical correlation analysis. *Computational Intelligence and Neuroscience*, 2018, 2018.

[64] Victor Javier Kartsch et al. A sensor fusion approach for drowsiness detection in wearable ultra-low-power systems. *Information Fusion*, 43:66–76, 2018.

[65] Simone Benatti et al. Multiple biopotentials acquisition system for wearable applications. In *BIODEVICES*, pages 260–268, 2015.

[66] Texas Instruments, 2015. URL `http://www.ti.com/lit/ds/symlink/ads1298.pdf`.

[67] Gene H Golub. Matrix decompositions and statistical calculations. In *Statistical Computation*, pages 365–397. Elsevier, 1969.

[68] Åke Björck and Gene H Golub. Numerical methods for computing angles between linear subspaces. *Mathematics of computation*, 27(123):579–594, 1973.

[69] MATLAB. *version 9.2.0 (R2017a)*. The MathWorks Inc., Natick, Massachusetts, 2017.

[70] ARM. CMSIS Library, 2016. URL `https://www.arm.com/products/processors/cortex-m/cortex-microcontroller-software-interface-standard.php`.

[71] David Regan. Recent advances in electrical recording from the human brain. *Nature*, 253(5491):401, 1975.

[72] Christoph S Herrmann. Human EEG responses to 1–100 Hz flicker: resonance phenomena in visual cortex and their potential correlation to cognitive phenomena. *Experimental brain research*, 137(3-4):346–353, 2001.

[73] Rafał Kuś et al. On the quantification of SSVEP frequency responses in human EEG in realistic bci conditions. *PloS one*, 8(10):e77536, 2013.

[74] J Vernon Odom et al. Visual evoked potentials standard (2004). *Documenta ophthalmologica*, 108(2):115–123, 2004.

[75] Nikolay V Manyakov et al. Sampled sinusoidal stimulation profile and multichannel fuzzy logic classification for monitor-based phase-coded ssvep brain–computer interfacing. *Journal of neural engineering*, 10(3):036011, 2013.

[76] Fabrizio Beverina, Giorgio Palmas, Stefano Silvoni, Francesco Piccione, Silvio Giove, et al. User adaptive bcis: Ssvep and p300 based interfaces. *PsychNology Journal*, 1(4):331–354, 2003.

[77] Yosuke Kimura, Toshihisa Tanaka, Hiroshi Higashi, and Naoki Morikawa. Ssvep-based brain–computer interfaces using fsk-modulated visual stimuli. *IEEE Transactions on Biomedical Engineering*, 60(10):2831–2838, 2013.

[78] Pablo F Diez et al. Asynchronous BCI control using high-frequency SSVEP. *Journal of neuroengineering and rehabilitation*, 8(1):39, 2011.

[79] Jiří Kárník and Jakub Streit. Summary of available indoor location techniques. *IFAC-PapersOnLine*, 49(25):311–317, 2016.

[80] Chouchang Yang and Huai-Rong Shao. Wifi-based indoor positioning. *IEEE Communications Magazine*, 53(3):150–157, 2015.

[81] Dempster Andrew G Lim Samsung Moghtadaiee, Vahideh. Indoor localization using fm radio signals: A fingerprinting approach. In *Indoor Positioning and Indoor Navigation (IPIN)*. IEEE, 2011.

[82] Janire Larranaga, Leire Muguira, Juan-Manuel Lopez-Garde, and Juan-Ignacio Vazquez. An environment adaptive zigbee-based indoor positioning algorithm. In *Indoor Positioning and Indoor Navigation (IPIN), 2010 International Conference on*, pages 1–8. IEEE, 2010.

[83] S. Liu, Y. Jiang, and A. Striegel. Face-to-face proximity estimationusing bluetooth on smartphones. *IEEE Transactions on Mobile Computing*, 13(4):811–823, April 2014. ISSN 1536-1233. doi: 10.1109/TMC.2013.44.

[84] Yuechun Chu and Aura Ganz. A uwb-based 3d location system for indoor environments. In *Broadband Networks, 2005. BroadNets 2005. 2nd International Conference on*, pages 1147–1155. IEEE, 2005.

[85] L. M. Ni, Yunhao Liu, Yiu Cho Lau, and A. P. Patil. Landmarc: indoor location sensing using active rfid. In *Proceedings of the First IEEE International Conference on Pervasive Computing and Communications, 2003. (PerCom 2003).*, pages 407–415, March 2003. doi: 10.1109/PERCOM.2003.1192765.

[86] Jaewoo Chung, Matt Donahoe, Chris Schmandt, Ig-Jae Kim, Pedram Razavai, and Micaela Wiseman. Indoor location sensing using geo-magnetism. In *Proceedings of the 9th international conference on Mobile systems, applications, and services*, pages 141–154. ACM, 2011.

[87] Qian Lu, Xuewen Liao, Shulin Xu, and Wei Zhu. A hybrid indoor positioning algorithm based on wifi fingerprinting and pedestrian dead reckoning. In *Personal, Indoor, and Mobile Radio Communications (PIMRC), 2016 IEEE 27th Annual International Symposium on*. IEEE, 2016.

[88] Ching-Chieh Chiu, Jen-Chieh Hsu, and Jenq-Shiou Leu. Implementation and analysis of hybrid wireless indoor positioning with ibeacon and wi-fi. In *Ultra Modern Telecommunications and Control Systems and Workshops (ICUMT), 2016 8th International Congress on*. IEEE, 2016.

[89] B. Rebsamen, E. Burdet, C. Guan, H. Zhang, C. L. Teo, Q. Zeng, C. Laugier, and M. H. Ang Jr. Controlling a wheelchair indoors using thought. *IEEE Intelligent Systems*, 22(2), March 2007. ISSN 1541-1672. doi: 10.1109/MIS.2007.26.

[90] M Shamim Hossain. Cloud-supported cyber–physical localization framework for patients monitoring. *IEEE Systems Journal*, 2015.

[91] IndoorAtlas. Homepage. `https://www.indooratlas.com/`.

[92] M. Tomasini, S. Benatti, B. Milosevic, E. Farella, and L. Benini. Power line interference removal for high-quality continuous biosignal monitoring with low-power wearable devices. *IEEE Journal*, 2016. doi: 10.1109/JSEN.2016.2536363.

[93] V. Kartsch, S. Benatti, D. Rossi, and L. Benini. A wearable eeg-based drowsiness detection system with blink duration and alpha waves analysis. In *8th International IEEE EMBS Conference on Neural Engineering*. IEEE, 2017.

[94] Richard W Homan, John Herman, and Phillip Purdy. Cerebral location of international 1020 system electrode placement. *Electroencephalography and Clinical Neurophysiology*, 66(4):376 – 382, 1987. ISSN 0013-4694. doi: https://doi.org/10.1016/0013-4694(87)90206-9.

[95] Yijun Wang, Zhiguang Zhang, Xiaorong Gao, and Shangkai Gao. Lead selection for ssvep-based brain-computer interface. In *Engineering in Medicine and Biology Society, 2004. IEMBS'04*. IEEE.

[96] Christoph Guger, Clemens Holzner, Christoph Grönegress, Günther Edlinger, and Mel Slater. Control of a smart home with a brain-computer interface. 2008.

[97] YONGWON Kim, NETIWIT Kaongoen, and SUNGHO Jo. Hybrid-bci smart glasses for controlling electrical devices. In *Society of Instrument and Control Engineers of Japan (SICE), 2015 54th Annual Conference of the*, pages 1162–1166. IEEE, 2015.

[98] Abdul Saboor, Aya Rezeika, Piotr Stawicki, Felix Gembler, Mihaly Benda, Thomas Grunenberg, and Ivan Volosyak. Ssvep-based bci in a smart home scenario. In *International Work-Conference on Artificial Neural Networks*, pages 474–485. Springer, 2017.

[99] EPSON. Moverio BT-200. `https://www.epson.it/products/see-through-mobile-viewer/moverio-bt-200`, 2018.

[100] Vuforia. Vuforia SDK for digital eyewear. `https://library.vuforia.com/articles/Training/Vuforia-for-Digital-Eyewear`, 2018.

[101] Danhua Zhu, Jordi Bieger, Gary Garcia Molina, and Ronald M Aarts. A survey of stimulation methods used in ssvep-based bcis. *Computational intelligence and neuroscience*, 2010:1, 2010.

[102] Davide Rossi, Francesco Conti, Andrea Marongiu, Antonio Pullini, Igor Loi, Michael Gautschi, Giuseppe Tagliavini, Alessandro Capotondi, Philippe Flatresse, and Luca Benini. Pulp: A parallel ultra low power platform for next generation iot applications. In *Hot Chips 27 Symposium (HCS), 2015 IEEE*, pages 1–39. IEEE, 2015.

[103] Nik Khadijah Nik Aznan, Stephen Bonner, Jason D Connolly, Noura Al Moubayed, and Toby P Breckon. On the classification of ssvep-based dry-eeg signals via convolutional neural networks. *arXiv preprint arXiv:1805.04157*, 2018.